Electrodeposition of Ni-Cu alloy electrodes in sulfate–citrate medium and their use for non-enzymatic glucose oxidation

Katia Hebbache, Nadia Ait Ahmed, Nabila Aliouane, Marielle Eyraud, Katia Mira, Aymene Achouri, Atmane Djermoune

Electrodeposition of Ni-Cu alloy electrodes in sulphate–citrate medium and their use for non enzymatic glucose oxidation

Katia. Hebbache[a], Nadia. Ait Ahmed[a] *, Nabila. Aliouane[a], Marielle. Eyraud[b], Katia. Mira[a], Aymene Achouri[a], Atmane Djermoune[c]

[a] *Université de Bejaia, faculté de Technologie, Laboratoire d'Electrochimie, de Corrosion et de Valorisation Energétique (LECVE), 06000 Bejaia, Algérie*
[b]*Aix-Marseille University, CNRS, MADIREL UMR 7246, équipe Electrochimie des Matériaux, 13397 Marseille Cedex 20, France*
[c]*Centre de Recherche Scientifique et Technique en Analyses physico-chimiques (CRAPC – Bejaia), Algérie*

*[a)] Address all correspondence to this author. e-mail: nadia.aitahmed@univ-bejaia.dz

Abstract

In this study, we present the use of a Ni-Cu alloy electrodeposited on a titanium electrode as a sensor for non-enzymatic glucose oxidation. Electrochemical parameters such as bath composition, potential and deposition times used to obtain the films, were studied. After optimization of operating conditions, the morphology, chemical composition and surface structure of the Ni-Cu alloy electrodes were characterized using scanning electron microscopy (SEM) coupled with energy dispersive X-ray (EDX) and X-ray diffraction spectroscopy (XRD). Electrocatalytic activity of the modified Ni-Cu electrodes towards non-enzymatic glucose oxidation was then evaluated by cyclic voltammetry, chronoamperometric and impedance spectroscopy. The experimental impedance data were fitted with an equivalent circuit model representing the electrode/electrolyte interface, to evaluate the charge transfer rate as well as the electrical characteristics of the catalytic surface. Cyclic voltammetry experiments show that the Ni-Cu films prepared at -0.975V for 10 min significantly generated the highest oxidation current, extended linear responses for glucose concentrations in the range of 0.25 to 8mM, with excellent values of the limit of detection (LOD: 4.97µM) and sensitivity (546 µA mM^{-1} cm^{-2}). Effects of endogenous interfering species (ascorbic acid (AA), uric acid (UA), oxalic acid, fructose, sucrose, NaCl and KNO_3) on the electrocatalytic response of Ni-Cu /Ti were also studied and showed that Ni-Cu /Ti is selective electrocatalyst towards glucose oxidation. The application of Ni-Cu/Ti biosensor in real human saliva and urine samples is demonstrated using chronoamperometric detection: the increase in current remains proportional to successive additions of glucose. Finally, it was shown that the Cu-Ni/Ti sensor presented the lowest charge transfer resistance (Rct) and the highest double layer capacitance values compared to those of the pure Ti, Ni/Ti and Cu/Ti electrodes. The improved electrocatalytic activity is mainly attributed by the synergistic effect between Ni and Cu.

Keywords: Glucose oxidation, NiCu alloy, Electrocatalysis, Cyclic voltammetry, Chronoamperometric

Introduction

In recent years, the identification and determination of glucose have been important issues that have attracted much attention in various fields such as clinical medical diagnostics, food industry analysis, biotechnology and fermentation **[1-3]**.

Glucose is the body's most important substance and main source of energy. It plays a crucial role in the functioning of the body, its hydrolysis leading to its storage in the form of glycogen. It can protect and detoxify the liver and promotes the metabolism of poisons **[4-11]**.

However, abnormal fluctuations in blood glucose, such as hypo glycaemia and hyper glycaemia, are dangerous to health **[5,6]** and can also lead to many adverse effects or serious problems that damage organs, particularly diabetes **[10,11]**. Diabetes is one of the leading causes of death worldwide **[9, 12]**.

Diabetes is a chronic metabolic disease characterized by persistent hyper glycaemia **[13]**, in which the pancreas cannot produce enough insulin to absorb and regulate glucose as an energy source **[14, 15]**. It is characterized by a high accumulation of glucose in the blood **[14-21]**, leading to other serious illnesses, such as kidney failure, stroke, blindness, loss of sight, heart disease, nerve damage, and finally an enormous financial burden **[14, 16-22]**. Diabetes has become a global public health problem **[23]**, according to a recent study by the World Health Organization (WHO) and the International Diabetes Federation (IDF). The study found that nearly 422 million people have diabetes, and by 2030 this number is expected to continue to rise rapidly to 642 million **[24, 25]**.

For these reasons, it is crucial to put in place monitoring, regulation and control measures that enable rapid and accurate detection of blood sugar levels. This is essential for the preservation of human health, the treatment of diabetes, and the prevention and reduction of complications associated with diabetes mellitus.

Much effort has gone into developing techniques for detecting and quantifying glucose levels [**26-27]** including colorimetry **[28, 29]**, chemiluminescence **[30],** fluorescence **[31-32]**, surface-enhanced Raman scattering **[33, 34]**, mass spectrometry **[35, 36]** and electrochemical methods **[22, 27, 37-42]**. This latter is considered the most practical and promising due to its excellent performance. Consequently, the development of electrochemical glucose sensors has attracted a great deal of interest in recent decades **[17, 22, 43-44]**.

Depending on the sensitive materials used, electrochemical glucose sensors are classified into two categories: enzymatic and non-enzymatic sensors **[15, 45-47]**.

To date, most sensors are based on catalytic enzymatic detection approaches, which offer superior selectivity but suffer from stability and storage problems **[14, 48-54]**. In order to overcome these limitations, alternative non-enzymatic sensors are currently being developed **[55-57].** These sensors are based on the direct oxidation of glucose at the electrode surface, offering excellent performance in terms of sensitivity, selectivity, long-term stability and low cost **[13, 25, 50-51, 54, 58-59]**.

According to previous studies, a wide variety of inorganic modified electrode materials have been used, including noble metals (Ag, Au, Pd and Pt) **[60-69]**, transition metals (Cu, Ni, Zn, Ti, Mn) **[3, 70-74]**, metal oxides (NiO, CuO, $NiCo_2O_4$) **[11, 13, 58, 75-89]** as well as alloys such as (Pt-Pb, Pt-Au, Cu-Co, Pt-Ni, Ni-Cu) **[90-97]**.

The study of alloy-based electrodes is motivated by the anticipation of an electrocatalytic synergy benefiting from the combined properties of the alloy components. Kuwana et al examined the oxidation of carbohydrates on Ni-based alloys **[96-98]**. They reported that Ni-containing alloys showed promising stability for glucose oxidation **[96, 99]**. Khulbe et al **[99]** explored the behavior of Ni-Cu alloy in various catalytic reactions, including hydrogenation reactions, conversion of hydrogen to orthoparasite and the H_2/D_2 exchange reaction **[96]**.

The novelty of our work lies in the absence of reports detailing the one step electrodeposition of Ni-Cu thin-film on Ti to promote a non-enzymatic glucose sensor. Specifically, the influence of various electrodeposition and detection parameters was studied including the impact of citrate complexing additive, electrodeposition potential and duration, pH levels, selection of detection medium, and their influence on the glucose oxidation. Our research has yielded novel findings demonstrating a significant enhancement in the electrocatalytic activity of Ni-Cu/Ti towards glucose oxidation, coupled with excellent conductivity.

The aim of this work was to study the electrocatalytic activity of non-enzymatic glucose on a nickel-copper alloy modified titanium electrode in an alkaline 0.1M KOH solution. Ni-Cu thin films were deposited on a Ti substrate from a 0.6 M $NiSO_4.6H_2O$, 0.03 M $CuSO_4.5H_2O$, in presence of citrate. The electrodeposition mechanism of the Cu-Ni alloy as well as the electrochemical behaviors of Ni^{2+} and Cu^{2+} ions, were investigated. Ni-Cu alloy coatings were electrodeposited by chronoamperometric method at different potentials and deposition times.
The effect of electrodeposition parameters on the detection of non-enzymatic glucose was performed using cyclic voltammetry, chronoamperometric and electrochemical impedance spectroscopy.

Experimental

1) - Materials and methods

Ni-Cu alloys were obtained onto titanium substrate (thickness 0.125mm, purity 99.6%, status annealed and size 100*100 mm^2). The electrolytes contained 0.6M $NiSO_4$ and 0.03M $CuSO_4$ (98.5% and 99% purity respectively, purchased from Biochem Chemopharma), with 1M Na_2SO_4 (99.9% purity, Analar) and 0.4M H_3BO_3 (99.5% purity, Biochem Chemopharma) as supporting salts. 0.15M Citrate salts were used as additives (99% purity, Sigma-Aldrich). The initial pH was adjusted at 3 with sulfuric acid. A classical three-electrode cell was used containing: a 2 cm^2 titanium substrate as working electrode, a platinum plate as counter-electrode and a calomel electrode saturated with potassium chloride (SCE) as reference electrode.
All potentials were indicated with respect towards SCE. Thin films were obtained by chronoamperometric method, at different potentials (-0.950V and -0.975V) for times ranging from 1 to 15 min, at room temperature. The resulting electrode was washed and air-dried.
Sodium citrate was chosen as complexing agent. It is known to reduce the difference between the deposition potential of Ni (E°=−0.25V/SHE) and Cu (E°=+0.34V/SHE) improving the deposition efficiency, achieving stress-free deposition even at very high current densities.
Boric acid acts as a buffer agent at the electrode surface: by decreasing the hydrogen evolution at the electrode surface, it helps to stabilize bath pH and prevent the formation of nickel and copper hydroxide precipitates on the substrate.
The electrochemical response of interfering species such as ascorbic acid (AA, 99.7% purity Biochem Chemopharma), uric acid (UA, purity >98% Fluka), oxalic acid (98% purity Prolabo), fructose (Fru, purity 99% Sigma Aldrich), sucrose (Suc, purity 99% Fluka), NaCl (100% purity Analar NormaPur) and KNO_3 (99% purity Biochem Chemopharma) was studied in the presence of glucose (99% purity Biochem Chemopharma) on the Ni-Cu alloy.

Glucose detection was also performed in two real human samples in 0.1 M KOH solution : in 1/10 diluted saliva and in a 1/50 collected urine sample. Chronoamperometric measurements were performed in these diluted real media and during the successive glucose additions to reach glucose concentrations of 0.5, 1 and finally 4 mM.

2) - Characterization

X-ray diffraction (XRD) analysis was carried out to study the phases of the crystal structure of the prepared sample Ni-Cu/Ti modified electrode coatings. The instrument used for this analysis was the XRD (Siemens D-5000 diffractometer) using incident Cu Kα radiation (λ = 1.5418 Å) within a scan rate of 0.04°.

The Scanning Electron Microscopy (SEM) analysis equipped with Energy Dispersive X-ray Spectroscopy (EDS) was performed to investigate the surface morphology and composition of Ni-Cu/Ti modified electrode. The instrument used for this analysis was SEM Zeiss Gemini SEM 500 70-04.

3) - Detection medium of glucose

Nickel-Copper alloys were used to study the non-enzymatic oxidation of glucose $C_6H_{12}O_6$ (99% purity, from Biochem Chemopharma) using electrochemical methods such as cyclic voltammetry, chronoamperometric and electrochemical impedance spectroscopy (EIS).

RESULTS AND DISCUSSION

Electrochemical measurements

Electrochemical measurement in supporting electrolyte on Ti

A preliminary cyclic voltammetry study of the supporting electrolyte consisting of Na_2SO_4 (1M) + H_3BO_3 (0.4M), enabled us to determine its stability range (**Figure 1 (a)**). 0.15M sodium citrate ($C_6H_5Na_3O_7$) was then added to the supporting electrolyte to see whether citrate undergoes electrochemical reactions (**Figure 1. (b)**). It appears clearly that no electrochemical reaction takes place at the electrode surface either with or without citrate, except the H^+reduction at -0,8V according to eq.1:

$2H^+ + 2e^- \longrightarrow H_2$ ……(eq.1)

Fig 1. : Cyclic voltammogram of titanium substrate immersed in: a) 1M Na_2SO_4 + 0.4M H_3BO_3 , b) 1M Na_2SO_4 + 0.4M H_3BO_3 + 0.15M $C_6H_5Na_3O_7$, pH 3 with V_b=8mV/s.

Electrochemical measurement in Ni, Cu and Ni-Cu containing solutions

Before moving on to the study of the Ni-Cu alloy, it was necessary to study the behavior of titanium substrate in the supporting electrolyte containing respectively Ni^{2+} or Cu^{2+} salts . The CV curve recorded from the electrolyte solution containing 0.6M $NiSO_4$ + 0.1M H_3BO_3 + 1M Na_2SO_4 + 0.15M $C_6H_5Na_3O_7$, pH=3 is shown in **Fig. 2a**. During the forward sweep, a cathodic current appears in region A, from a potential of about -0.7V with a current density of -0.15mA/cm^2, corresponding to the reduction of nickel, followed by a significant increase in current at more negative potentials due to the H^+ reduction.

On the backward sweep, the little oxidation peak referred as B at approximately -0.14V with a current density of 0.67mA/cm^2 is linked to the dissolution of the single Ni phase already formed previously **[100]**. This behavior has been observed in the literature during the electrodeposition of nickel on different substrates **[101, 102]**.

Fig. 2b shows the voltammetric response of a solution of 0.03M $CuSO_4$ + 0.1M H_3BO_3 +1M Na_2SO_4+0.15M $C_6H_5Na_3O_7$, pH =3. During the cathodic scan, a single reduction peak referred as A is observed at approximately -0.370V, corresponding to a current density of -2.3mA/cm^2. This feature is indicative of the copper reduction process on the Ti surface. A limiting current is performed for a potential range between -0.6 to -0.8V, showing that the copper reduction is under mass transfer control. During the backward scan, a crossover is performed

between the forward and the backward currents. This overpotential is due to the nucleation and growth process induced by the electrodeposition of a metal on a foreigner substrate. At higher potentials, an intense anodic peak B appears at about 0.11V, resulting from the dissolution of the copper deposit formed during the cathodic scan. This is in agreement with a previous study for copper deposition on the FTO substrate **[103]**.

Fig. 2 Cyclic voltammogram of Ti in: (a): 0.6M $NiSO_4$+0.1M H_3BO_3 +1M Na_2SO_4+0.15M $C_6H_5Na_3O_7$. (b): 0.03M $CuSO_4$ +0.1M H_3BO_3 +1M Na_2SO_4 +0.15M $C_6H_5Na_3O_7$, V_b =8mV/s, pH=3.

Figure 3. (a) shows voltammograms on the titanium electrode immersed in citrate solutions containing Ni^{2+} ions (Ni^{2+} 0.6M 0.1M H_3BO_3 +1M Na_2SO_4+0.15M $C_6H_5Na_3O_7$), Cu^{2+} ions (0.03M Cu^{2+} + 0.1M H_3BO_3 +1M Na_2SO_4+0.15M $C_6H_5Na_3O_7$) or both Ni^{2+} and Cu^{2+} ions (Ni^{2+} 0.6M+ 0.03M Cu^{2+} + 0.1M H_3BO_3 +1M Na_2SO_4+0.15M $C_6H_5Na_3O_7$). During the initial scan, a cathodic current was observed from -0.150V attributed to the start of Cu^{2+} reduction. A broad cathodic reduction peak (referred as peak A) is then observed at -0.320V, similar to what was observed in the Cu electrolyte alone. This could be associated with the preferential cathodic reduction of Cu^{2+} ions in the Ni-Cu electrolyte **[104]**. When a normal co-deposition mechanism is involved, the more noble metal, namely copper here, is reduced to more positive potentials than the less noble metal (here nickel) **[105]**. This also indicates that during copper electrodeposition, the charge transfer step is rapid, and the growth rate is controlled by the Cu^{2+} diffusion from the in solution to the nucleation sites at the titanium electrode surface. A low concentration of Cu^{2+} ions in solution suggests that deposition is diffusion controlled over a wide potential range from -0.46V to the onset of Ni deposition at around -0.7V, referred as B on the curve **[104]**. Thus, Ni is deposited on a Cu pre-coated substrate and requires less energy than on a bare titanium surface, indicating that incorporation of significant amounts of Ni into the deposits occurs rapidly over a relatively narrow potential range **[105]**. This is followed by a significant increase in current at more negative potentials due to proton reduction, corresponding to the disappearance of the nickel reduction peak, which is justified by the hydrogen evolution reaction.

In the backward scan, two intense anodic peaks (referred as C and D) are observed at 0.13 and 0.20V. The first peak is attributed to the copper oxidation because it is located as the same potential than that obtained for Cu alone in solution. The second peak can be attributed to the dissolution of the Ni-Cu alloy. **[100]**. It should be noted that, when Ni is alone in solution, nickel dissolution starts at potentials above - 0.14V, but in presence of Cu, there is no nickel dissolution alone. This feature clearly shows the incorporation of Ni into the copper deposit; the double oxidation peak indicating a two-phases Cu / CuNi deposit with different chemical compositions.

Figure 3 (b) shows the effect of citrate on the kinetics and mechanism of Ni-Cu alloy formation, with a decrease in the current densities of the anodic and cathodic peaks in presence of citrate.

According to the results of the CV study, an appropriate range of current densities is chosen for the subsequent deposition of Ni-rich Ni-Cu alloys **[105]**.

Fig. 3 Cyclic voltammogram on a titanium electrode in an electrolyte containing (a): 0.6M $NiSO_4$ + 0.03M $CuSO_4$ + 0.1M H_3BO_3 + 1M Na_2SO_4 + 0.15M $C_6H_5Na_3O_7$ (b): 0.6M $NiSO_4$ + 0.03M $CuSO_4$ + 0.1M H_3BO_3 + 1M Na_2SO_4 without citrate, V_b=8mV/s at pH=3.

Chronoamperometric investigations

Fig.4 shows the chronoamperometry of Ni-Cu composite deposits, obtained at -0.950 and -0.975V for 7min and 10min electrodeposition times respectively. The Ni-Cu system is considered to be of the normal codeposition type according to Brenner's classification **[106]**.

The transients present a rapid increase in cathodic current density, followed by a stable value. This increase in current density is linked to the formation and growth of Ni-Cu nuclei, as well as the increase in the number of these nuclei on the electrode. This step is not followed by a decrease in current due to the diffusional control of the reaction as could have been obtained, for example, in the case of pure copper reduction. Indeed, the deposition potentials are located in the region where not only Cu^{2+}, but also Ni^{2+} and H^{+} reductions can occur, the last two being under charge transfer control. The current density stabilizes at a higher value in the transient obtained at -975mV, compared to that at -950mV, which is in agreement with the CV study.

This means that the potential applied during deposition of the copper-nickel alloy influences the rate of nucleation towards the active sites on the electrode surface.

Fig. 4 Chronoamperometry of Ni-Cu/Ti deposits obtained at: (a) -0.95V for 7min and (b) -0.975V for 10min.

Morphological and structural characterization

Fig.5 (a, b and c) shows the SEM images of Ni-Cu/Ti deposits obtained at [-0.975V for 10min]. The surface is covered with homogeneous and compact deposit, composed of a mixture of spherical aggregates forming a cauliflower morphology, with grains in the nanometer range. In addition, a smooth and uniform distribution of the Ni-Cu alloy on the Ti surface was also observed. On the other hand, pure Ni and Cu deposits **in Fig.5 (d, e, f and g)** presented spherical shapes. The Ti substrate is not entirely covered by the pure deposits, even for the pure Ni film obtained in the same conditions than the Cu-Ni alloy. The surface morphology of the alloy is consistent with the creation of more active sites for the electrochemical reaction, thus enhancing the electrocatalytic activity of the nanoparticles through more efficient electron transfer between the analyte and the electrode.

It is also important to note that the Ni-Cu morphology is highly dependent on deposition potentials, a potential of -0.950V (**figure 5. h**) leading to a rougher deposit composed by larger grains than those obtained at -0.975V.

Fig. 5 (a, b, c) SEM images of Ni-Cu/Ti deposit obtained at -0.975V for 10min, (d, e): SEM images of Ni/Ti deposit obtained at -0.975V for 10min, (f, g): SEM images of Cu/Ti deposit obtained at -0.370V for 10min and (h): Ni-Cu/Ti deposit obtained at -0.950V for 10min.

Aïda Varea et al (2012) succeeded in obtaining a cauliflower-shaped deposition surface on a substrate composed of adhesion layers and electric beam evaporated Ti (25 nm)/Cu (250 nm) seeds **[104]**. In comparison with the work of Umut Sarac et al (2013) **[107]**, they made SEM images of Ni-Cu films grown on ITO substrates deposited at different electrolyte temperatures. These images revealed the microstructure of the films, showing compact surfaces free from cracks. The SEM images clearly show an increase in cluster formation with increasing electrolyte temperature. In comparison, the surface of films deposited at an electrolyte temperature of 25°C is more uniform than films deposited at higher electrolyte temperatures.

The **Figure 6a** shows an image at a magnification of 5µm on a Ni-Cu/Ti sample deposited during 10 min at -0.975V, and the corresponding the EDX spectrum (**Fig.6b**). EDX analyse carried out on the entire surface of the figure, shows the presence of Ni and Cu in proportion of 44 and 56 wt % respectively.

Fig. 6 (a) SEM images of Ni-Cu/Ti deposit obtained at -0.975V for 10min, (b) EDX analysis of Ni-Cu/Ti obtained at -0.975V for 10min.

Figure 7 shows XRD diffractograms of Ti, Ni/Ti [-0.975V, 10min], Cu/Ti [-0.370V, 10min], and Ni-Cu [-0.975V, 10min], as well as Ni-Cu/Ti [-0.975V, 10 min]. These diffractograms were indexed against CFC structure, revealing the presence of characteristic lines for Cu (see JCPDF 04-836) in **Figure 7(c)**, Ni (see JCPDF 65-2865) in **Figure 7(b)**, and the Ni-Cu alloy (see JCPDF 65-7246) in **Figure 7(d)**. In this diagram, some additional diffraction peaks can be seen, attributed to the titanium substrate (see JCPDF 44-1294), indicating the thinness of the Ni-Cu coating.

It has been established that Ni and Cu exhibit CFC gratings with similar lattice parameters, forming a solid solution across the entire phase diagram **[104]**.
The three characteristic diffraction peaks (111), (200), and (220) observed at 44, 51.25, and 74.1 degrees were assigned to the CFC crystals of the Ni-Cu alloy, respectively **[94, 108]**. The (111) crystallographic plane shows a maximum intensity compared with the other deposition planes studied **[109]**, attributable to the incorporation of Cu atoms into the Ni lattice. That result can explained the change in surface morphologies obtained between the pure Cu and Ni deposits and the alloy **[104]**.

Fig. 7 X-ray diffractograms of (a): Ti, (b): Ni/Ti, (c) Cu/Ti and (d) Ni-Cu/Ti.

Electrochemical behavior of Ti, Ni/Ti, Cu/Ti and Ni-Cu/Ti towards the non-enzymatic oxidation of glucose

Figure 8(a) shows cyclic voltammograms on the various electrodes, namely Ti, Ni/Ti, Cu/Ti and Ni-Cu/Ti, in KOH medium. Measurements were carried out in the potential range [-0.2V; -0.750V] at a sweep rate (V_b) of 8 mV/s. On Ti substrate no current was detected, while on Cu/Ti electrode there was an anodic current corresponding to the water oxidation for potentials higher than 0,6V. No other reaction was observed on these electrodes, since no other anodic or cathodic peaks were detected.
However, for the Ni electrode, anodic and cathodic peaks referred as A and B were observed at 0.42V and 0.35V respectively. These peaks are less intense than those observed for the Ni-Cu alloy (see peaks C and D). They can be attributed to the formation of nickel hydroxide ($Ni(OH)_2$) in KOH medium, corresponding to the Ni(II)-Ni(III) redox couple, on both electrodes. This process involves the formation of NiOOH, as described by equations (2 and 3), as reported in the literature **[89, 94-95, 110-114]**.
According to the electron transfer which occurs in an alkaline medium, the mechanism of the electrochemical reaction can be proposed as follows:

$$Ni + 2OH^- \rightarrow Ni(OH)_2 + 2e^- \qquad (eq.2)$$

$$Ni(OH)_2 + OH^- \rightarrow NiOOH + H_2O + e^- \qquad (eq.3)$$

These experimental results are consistent with some works reported in the literature **[94, 95, 110]**.

Figure 8 (b) shows the voltammograms recorded on different electrodes in the 5mM glucose + 0.1M KOH detection medium. No significant response is observed for the bare titanium electrode, unlike other electrodes for

which large anodic peaks can be observed for potentials higher than 0.2V. They correspond to the non-enzymatic oxidation of glucose ($C_6H_{12}O_6$). The intensity of these peaks increases gradually going from Cu (referred as A), Ni (referred as B) and Cu-Ni (referred as C) electrodes.

This increase in current intensity can be attributed to the synergistic and electronic effect between Ni and Cu generated by the $Ni(OH)_2/NiOOH$ and $Cu(OH)_2/CuOOH$ couples at the electrode surface, in reaction with glucose **[96, 115]**. Similar results were observed by Saman Nisar, and Ji-Eun Lim and M. Jafarian, who studied the electrochemical oxidation of glucose on Ni-CuNPs@VC/GCE, Ni_x-Cu_y/GCE and Ni-Cu/GCE electrodes respectively **[94-96]**.

According to previous works **[94-95]**, **[98, 110-113]**, **[116-123]**, it is widely accepted that in 0.1 M KOH solution, the mechanism can be simply summarized as follows: Ni is first oxidized *Ni(II)* in (eq. (3)), which is then oxidized in *Ni(III)* (*eq. 4*). Glucose molecules are first adsorbed onto the Ni-Cu active sites to be oxidized to gluconolactone ($C_6H_{10}O_6$) at higher potentials, with the simultaneous reduction of $Ni(III) in\ Ni(II)$ according to equatios ($eq.5$). The same mechanism can be applied for Cu, oxidized into $Cu(II) and\ then\ Cu(III)$ species according to equations ($eq.5$- $eq.6$- $eq.7$). In this way, the Ni-Cu surface layer can be transformed into a mixture of redox couples $Ni(OH)_2/NiOOH$ and $Cu(OH)_2/CuOOH$. Therefore, the possible process of non-enzymatic glucose oxidation on the surface of Ni-Cu/Ti nanoparticles can be simply summarized by the following reactions **[115, 121, 124]**:

$$Ni + 2OH^- \rightarrow Ni(OH)_2 + 2e^- \qquad (eq.2)$$

$$Ni(OH)_2 + OH^- \rightarrow NiOOH + H_2O + e^- \qquad (eq.3)$$

$$2NiOOH + glucose \rightarrow 2Ni(OH)_2 + gluconolactone \qquad (eq.4)$$

$$Cu + 2OH^- \rightarrow Cu(OH)_2 + 2e^- \qquad (eq.5)$$

$$Cu(OH)_2 + OH^- \rightarrow CuOOH + H_2O + e^- \qquad (eq.6)$$

$$2CuOOH + glucose \rightarrow 2Cu(OH)_2 + gluconolactone \qquad (eq.7)$$

The general mechanism proposed:

$$2\ \ NiOOH + 2CuOOH + 2glucose \rightarrow 2Ni(OH)_2 + 2Cu(OH)_2 + 2gluconolactone \qquad (eq.8)$$

Figure 8(c) performed on Ni-Cu/Ti, highlights the significant increase of the oxidation peak, after the addition of glucose into the KOH solution.

Fig. 8 Cyclic voltammograms obtained on the different deposition electrodes: Ti, Ni/Ti, Cu/Ti, Ni-Cu/Ti, (a): 0.1M KOH without addition of glucose, (b): in 5mM glucose + 0.1M KOH, (c): comparison of the curves previously obtained on Cu-Ni/Ti electrode with and without glucose; pH=13, V_b=8mV/s.

Choice of detection medium

The influence of the medium on the electrocatalytic activity Cu-Ni/Ti electrode (E= -0.975V at t= 10min) was studied. The comparison of the voltammetry results obtained in (0.1M KOH + 5mM Glucose, pH 13), (0.1M PBS (0.1M K_2HPO_4 + 0.1M KH_2PO_4) + 5mM Glucose, pH 7.1) and (0.2M KCl + 5mM Glucose, pH 9), is shown in **Figure 9**. There was no significant response of glucose on the Ni-Cu/Ti modified electrode in PBS medium as well as in KCl solution. For this reason, a KOH medium with a concentration of 0.1M was finally chosen for the preparation of non-enzymatic glucose solutions for the further works.

Fig. 9 Cyclic voltammogram for the Ni-Cu/Ti deposit obtained [-0.975V 10min] in different media: 5mM Glucose +0.1M KOH, 5mM Glucose+0.2M KCl and 5mM Glucose+0.1M PBS (0.1M K_2HPO_4 + 0.1M KH_2PO_4), Vb=8mV/s.

Influence of time and potential used for Cu-Ni deposition.

The voltammograms in **figure 10 (a, b)** show that the electrodeposition time has a major influence on the electrocatalytic response to glucose oxidation. The CV curves in **fig.10 (a)** and **fig.10 (b)** are performed on Cu-Ni/Ti obtained at -950mV and -975mV respectively, for deposition times ranging from 1min to 15min. The higher current densities for the glucose oxidation reaction are respectively for a deposition time of 7min at -950mV and 10min at -975mV. **Fig.10 (c)** compares the highest intensity curves for each potential. The best electrocatalytic activity for glucose oxidation is obtained at -0.975V and a deposition time of 10 min, since the intensity of the oxidation peak referred as B is the highest. This is why 10 minutes was chosen as the optimum deposition time. For deposition times lower than 10 min, the accumulation of active Ni-Cu sites is insufficient; when the deposition time increases the excess Ni-Cu reduces the electron transfer **[114]**.

Fig. 10 Cyclic voltammograms of Ni-Cu/Ti in (5mM glucose+0.1M KOH, pH=13) at different deposition times and potentials (a): -0.950V, (b): -0.975V and (c): superposition of the highest intensity curve with obtained for each potential, V_b=8mV/s.

Effect of citrate in Cu-Ni deposition bath

Figure 11 shows the cyclic Ni-Cu/Ti voltamperograms recorded in presence and absence of citrates in Cu-Ni deposition bath. It is obvious than in presence of citrate, the deposit exhibits a higher oxidation peak (referred as A). The increase in the electrocatalytic activity towards glucose oxidation is probably due to an higher concentration of the pairs $Ni(OH)_2/NiOOH$ and $Cu(OH)_2/CuOOH$ on the electrode

Fig. 11 Cyclic voltammogram in 5mM glucose+0.1M KOH solution at pH=13 obtained on Ni-Cu/Ti deposited at (-0.975V, 10min and pH=3), (a): in absence of citrate, (b): in presence of citrate.

Effect of pH of the Cu-Ni bath

The pH of the Cu-Ni solution was varied from 3.0 to 5.0, in order to determine the optimum range for the electrocatalytic oxidation of glucose on the Ni-Cu/Ti modified electrode. **Figure 12** shows that the best electrocatalytic response is recorded for pH 3 with a high current intensity of 3.8 mA/cm^2 compared to those performed at pH 4 and 5. It is concluded that the pH effect affects electrocatalytic activity. Consequently, pH 3.0 was employed in subsequent studies.

Fig. 12 Cyclic voltammograms in 5mM glucose+0.1M KOH from pH= 13, for Ni-Cu/Ti films deposited at [-0.975V, 10min] at different pH= (3, 4 and 5), V_b=8mV/s.

Effect of glucose concentration in the detection bath

The effect of the glucose concentration contained in the detection bath, on the Ni-Cu/Ti electrode voltamperometry responses was shown in **Figure 13**.

Figure 13 (a) shows the voltamperograms obtained on the Ni-Cu/Ti electrode, for glucose concentrations varying from 0.25 to 8 mM. The anodic peak current for the glucose oxidation increases linearly with its concentration in solution with a correlation coefficient of 0.997 (**Fig.13 (b)**). It is noticeable that the correlation coefficient value obtained on Ni-Cu/Ti is higher compared to the values cited in the literature by Saman Nisar et al **[94],** done on a Ni-Cu NPs @VC/GCE electrode with R^2= 0.985. This difference may be due to the detection medium, the nature and morphology of the Ni-Cu/Ti electrode.

Fig. 13 (a) Cyclic voltammograms of Ni-Cu/Ti deposited at [-0.975V, 10min and pH=3] at different glucose concentrations in 0.1M KOH, pH=13, V_b=8mV/s **(b):** Variation of the maximum of the oxidation peak obtained in (a) as a function of the glucose concentration.

Thanks to **figure 13 (b)** and equation (9) written below**,** it is possible to determine the limit of detection (LOD) using the following equation:

$$LOD = (3.3\ SDV)/b \quad \ldots\ldots\ldots\ldots \quad .(eq.9)$$

Where SDV represents the standard deviation for 10 repetitions of cyclic voltammetry performed in the 0.1 M KOH blank solution and is estimated to 8.23 $*10^{-4}$ mM^{-1} cm^{-2}; b is the slope of the linear regression obtained from the calibration curve of the variation in glucose concentrations.

The LOD value obtained is around 4.97 µM, in the same order than those determined in the literature. The Ni-Cu sensor suggests good glucose detection, this result indicating that Ni-Cu/Ti is a promising candidate for the development of new non-enzymatic glucose sensors **[94, 125].**

The sensitivity deduced from the slope of the linear equation in Fig.13 (b) was 546 µA mM^{-1} cm^{-2} for glucose concentrations between 0.25 and 8mM.

Effect of the scan rate used for glucose oxidation CV curves

We monitored the influence of the scan rate on the glucose oxidation current in order to assess the kinetics and nature of the electrochemical process at the Ni-Cu/Ti interface. As shown in **Figure 14 (a)**, increasing the scan rate from 3 to 100 mV/s results in a shift of the glucose oxidation peak towards more anodic potentials and an increase of current densities.

On the other hand, during the backward scan, small reduction peaks appear at high scan speeds. Gluconolactone species produce during glucose oxidation don't have enough time to diffuse far from the electrode and are reduced when the scan is reversed.

Figure 14 (b) shows the variation of the anodic peak currents obtained in **Fig.14 (a)** as a function of the square root of the scan rate. The current evolution of the glucose oxidation peaks increases linearly with the square root of the scan rate, with a correlation coefficient of 0.997; the electrochemical oxidation of glucose at the electrode surface is then under a diffusion-controlled process, probably slower than the electro-oxidation of Ni-Cu/Ti electrode itself **[96]**.

Fig. 14 (a) Cyclic voltammograms on Ni-Cu/Ti film deposited at [-0.975V, t=10min, pH=3] in 5mM glucose + 0.1M KOH, pH=13, at different scan rates, (b) variation of the anodic peak current obtained in (a) as a function of the square root of the scan rate.

Test of electrocatalyst stability of the Cu-Ni/Ti electrode

To test the stability of the electrocatalyst, 250 potential sweep cycles were performed on the same Cu-Ni/Ti electrode, at a constant sweep rate of 20 $mV.s^{-1}$, in 5 mM glucose + 0.1M KOH electrolyte (**Figure 15**). The current densities for the electro-oxidation of glucose appear almost constant over the 250 cycles, indicating the stability of the electrocatalyst **Fig 15 (a)**. This result can be better seen in **figure 15 (b)** where the maximum of the oxidation peaks in **figure 15 (a)** has been plotted for each cycle, showing quite constant values.

Fig. 15 (a) Stability of the electrocatalyst for 275 potential sweep cycles performed in 5 mM glucose + 0.1 KOH, 20 mV s^{-1}. **(b)**: Histogram of maximum of the current intensity peaks obtained in (a) over the different cycles.

Chronoamperometric detection of glucose

Fig. 16 (a) shows double step choronoamperograms for the Ni-Cu/Ti in the presence of glucose over a concentration range of 0.25 to 8Mm, with applied potential steps of 560 and 250 mV, respectively. These potentials are located in the oxidation and reduction peaks obtained in the figure 16 (a).

The beginning of the curves shows a rapid decrease in current at the start of the process oxidation, followed by its stabilization at higher values as the concentration of glucose in solution is high. After 180s, the potential is switch towards the cathodic region of the corresponding CV curves. The currents performed are negligible, indicating an irreversibility of the glucose oxidation process**.**

Fig.16 (b) presents the variations of i = f (t-1/2) obtained short times in the decreasing parts of figure 16(a). Indeed, when the reaction is under mass control, this curve follows a linear behavior according the Cotrell's law [12**]**.

$$i(t) = n.\ F.\ C.\ D^{1/2}.\ \pi^{-1/2}.\ t^{-1/2} \qquad \text{(eq.10)}$$

With: i (t): current density ($A.cm^{-2}$), n: Number of electrons exchanging glucose case is 1, D: diffusion constant ($cm^2.s^{-1}$), C: concentration (mol/cm^3), F: Faraday's constant (96500 C), t: time (s)

The dominance of a diffusion-controlled process appears evident for all concentrations in glucose in solution, especially, in **Fig 16 (c)**, plotted for our nominal 5mM glucose concentration. From the slope of the line obtained, the value of the calculated diffusion coefficient is $8.8*10^{-5}$ cm^2/s with a correlation coefficient of 0.998. This result is in the same order of magnitude than that obtained by M. Jafarian et al [96] on a Ni-Cu/glassy carbon electrode: D = 1× 10-5 cm2. s-1. The difference may be due to the medium used in that case: 0.1 KOH + 5Mm glucose.

Fig. 16 (a) double steps chronoamperograms recorded at different glucose concentration in 0.1M KOH solution, pH=13, on Ni-Cu/Ti film deposited at [-975mV, t=10min, pH=3], at imposed potentials (E_1= 0.560V 180 sec, E_2=0.250V 100 sec, (b): Cottrell curve plotted from the first 25 s of the chronoamperograms obtained in (a), (c): Linear fit of the Cottrell curve plotted from the chronoamperogram of 5mM glucose + 0.1M KOH

Selectivity of the Ni-Cu/Ti electrode towards glucose

Selectivity is an important parameter towards sensors. It provides information on the possibility of detecting only the analyte of interest in a mixture.

As part of the study of sensor selectivity, glucose was oxidized at 0.560V in the presence of interfering species. In **figure 17**, the amperometric response is recorded on the Ni-Cu/Ti electrode in the 0.5 mM glucose + 0.1 KOH, by gradually adding every 5 minutes an interfering specie, namely ascorbic acid (AA), uric acid (UA), oxalic acid (OA), fructose, sucrose, NaCl and KNO_3 before adding again 0.5 mM of glucose at the end. The interferent concentration was 0.01 mM, much lower than that of glucose in the solution, as it can be in human body **[126].**

The results clearly show that additions of interferent species do not change the glucose oxidation current, indicating that the Cu-Ni/Ti electrode possess an excellent selectivity**.**

Fig. 17: Amperometric response of Ni-Cu/Ti electrode to injection of 0.5mM glucose followed by addition of 0.01mM interference species AA, Ur, oxalic acid, Fru, Sucr, NaCl and 0.5mM glucose recorded at 300s intervals in 0.1M KOH solution at 0.560V.

Glucose detection in real human saliva and urine

To assess the feasibility of the prepared sensor in real sample analysis, glucose detection in human saliva and urine samples was investigated using the Ni-Cu/Ti electrode sensor. Ten-fold diluted saliva was added to a 0.1M KOH solution and human urine sample collected was diluted in a 1:50 ratio with KOH 0.1 M solution. The i-t responses at 0.56V/ESC in saliva or urine containing solutions, were performed for successive glucose additions to reach concentrations of 0.5, 1 and finally 4 mM (see **figure 18 (a) and (b) respectively)**. In both media, the current response increases progressively with each successive glucose injection, to reach the same values than those obtained previously (**see Fig.16**). No noticeable change in the anodic current density was performed in presence of saliva and urine, the electrode keeping its rapid detection. These results suggest that the high performance of the Ni-Cu/Ti sensor is maintained, that sensor can be then used for glucose detection in real saliva and urine samples.

Fig. 18: Amperometric response of Ni-Cu/Ti electrode in 0,1 M KOH + 10% saliva (a) and in 0,1 M KOH + 2% urine respectively, followed by glucose additions every 300s to reach [0.5, 1 and 4mM] concentrations of glucose in solutions. E=0.56V/SCE

Impedance spectroscopy characterization

Electrochemical impedance spectroscopy experiments were performed on Ti, Cu/Ti, Ni/Ti and Ni-Cu/Ti in a 5mM glucose + 0.1M KOH solution, at a potential of 0.56V with an amplitude of 10 mV, in the frequency range between 100 KHz and 10 MHz. The impedance diagrams of the Nyquist plots are shown in (**Figure. 19 (a), Figure.19 (b)** is a magnification of **Figure.19 (a)**). They show an imperfect single capacitive loop corresponding to a process limited by an electron transfer step during the electrocatalytic oxidation of glucose. The smaller the diameter of the semicircle, the greater the glucose oxidation reaction will be. The decrease in the semi-circle diameter in

function of surface varies in the order Ti > Cu/Ti > Ni/Ti > Ni-Cu/Ti. That confirms the electrocatalytic activity of this alloy with respect to glucose oxidation, in good agreement with voltammetry results. A simple equivalent circuit consisting of a solution resistance (Rs) in series with a parallel circuit of a constant phase element (CPEdl) and a polarization/charge transfer resistance (Rct) (**Figure 19 (c**)) has been employed to fit the EIS data for glucose oxidation. The CPE is used, because the formed double layer does not usually present an ideal capacitance behavior; its impedance is expressed as:

$$Z_{CPE} = \frac{1}{Y_0(J\omega)^n} \quad \text{(eq.11)}$$

Where Y_0 is the admittance constant, j is the imaginary number, ω is the angular frequency (ω = 2πf) and n is the exponent of CPE. The n value, which varies from 0 to 1, depends on the surface roughness and heterogeneity because of the non-uniform current distribution. The n value can determine the nature of the electrochemical element; the element is an ideal capacitance if n = 1. The corresponding results processed with the impedance fitting software ZSimpWin, are reported in **Table 1**. The mean Rs value is about 32 ± 5 Ω.cm^2, the electrolyte being conductive thanks to the high KOH concentration. The Rct obtained on bare Ti is clearly higher than those on Cu and Ni respectively. The lowest value was determined on the modified Cu-Ni/Ti surface showing a synergetic effect between Ni and Cu for glucose oxidation as well as a good electrical conductivity **[127].** It should also be noted that the capacitance of the Ni-Cu/Ti double layer is 3494 µF.cm^{-2}, which is the highest value, showing again the synergetic effect between Ni and Cu.

Fig. 19 (a) and (b) Nyquist and Bode diagrams respectively of the different electrodes: Ti, Cu/Ti [-0.370V 10min], Ni/Ti [-0.975V 10min] and Ni-Cu/Ti [-0.975V 10min] at an applied potential of 0.56V in 5mM glucose + 0.1M KOH with comparison of experimental data (scatter) and fit data (black line), **(c)**: Equivalent electrical circuit model for glucose oxidation in basic medium on Ni-Cu/Ti modified electrode used to fit experimental impedance data

Table.1: EIS parameters obtained by adjusting the Nyquist of different electrodes in a 0.1M KOH solution in the presence of 5 mM of glucose at room temperature at an applied oxidation potential of 0.56V:

Various electrodes	Rs (Ω.cm^2)	CPE (µF.cm^{-2})	Freq power n	Rct (Ω.cm^2)
Ti	37	16.7	0.95	4.53*10^4
Cu	32	249	0.83	952
Ni	32	302	0.95	336
Ni-Cu	29	3494	0.87	249

Effect of the glucose concentration on EIS measurements performed on Ni-Cu/Ti electrode.

The electrochemical impedance diagrams were recorded on the Ni-Cu/Ti electrode [-0.975V 10min] in a basic 0.1M KOH medium for different glucose concentrations [0.25- 8mM] at an imposed oxidation potential of 0.56V in Nyquist and Bode-phase plots. The results are shown in **Figure 20 (a and b).**

Figure 20.a shows the Nyquist diagram, comprising imperfect semicircles with a single high-frequency capacitive loop corresponding to the first process limited by an electron transfer step of glucose oxidation. The diameters of the semicircle and then the charge transfer resistance, vary inversely with the glucose concentration. This decrease indicates a good interaction between the glucose and the Ni-Cu layer **[127, 9]** and is characterized by the adsorption of glucose on the modified electrode. An equivalent result can be deduced from the impedance modulus |Z| obtained at low frequency in the **Figure 20 (b):** when the glucose concentration increases, the value of |Z| at low frequency decreases significantly. At the same time, the phase angle curves θ present a single peak that indicates that the oxidation involves a single constant, which corresponds to the charge transfer reaction, meaning that the glucose oxidation is the main process.

Fig. 20 (a) and **(b)** Nyquist and Bode diagrams respectively of the Ni-Cu/Ti electrode [-0.975V 10min], at different glucose concentrations compared with experimental data (scatter) and fit data (black line)

The values of the electrochemical impedance parameters obtained by fitting the data are presented in **Table 2**, showing that the Rct values decrease significantly with increasing variation in glucose concentration indicating that glucose oxidation occurred at a higher rate.

Table.2: EIS parameters obtained by adjusting the Nyquist of the modified electrode in a 0.1M KOH solution in the presence of different concentrations of glucose at room temperature at an applied oxidation potential of 0.56V.

[Glucose] mM /Parameters	$R_s(\Omega.cm^2)$	CPE ($mF.cm^2$)	Freq power n	R_{ct} ($\Omega.cm^2$)
0.25	28.2	2.34	0.81	737
0.5	28.5	2.87	0.83	674
1	29.6	2.93	0.85	621
2	30	3.31	0.85	564
3	32.5	3.66	0.87	428
4	28.6	3.20	0.86	308
5	28.7	3.49	0.87	249
6	29.5	3.74	0.85	196
7	29.1	3.83	0.84	134
8	29.8	3.65	0.83	106

These results indicate that Ni-Cu/Ti can be used as an electrochemical sensor for glucose detection, which is consistent with and confirmed by the voltammetry cyclic and chronoamperometry results.

On the other hand, the CPE values were not influenced by the increase in glucose concentration, nor the electrolyte resistance values (Rs), because the glucose concentrations remain very low **[9].**

Conclusion

In conclusion, Ni-Cu alloy films were successfully electrodeposited on Ti substrate from a bath containing nickel and copper sulfates in a boric acid media. The beneficial role of citrate added in the electrolyte was studied as well as the effects of pH, potential and duration on the surface morphology, structure, chemical composition and

electrochemical properties of the Ni-Cu/Ti sensor towards the glucose oxidation. Thanks to these preliminary studies, the best sensor was obtained for a potential of -0.975V applied for 10min. We also focused on the detection bath, a good electrocatalytic activity for glucose oxidation being determined in KOH media. In addition, this sensor demonstrated fast response time, high sensitivity and stability in the 0.25-8 mM concentration range. It was found to be a convenient and effective electrochemical sensor for glucose oxidation. The modified electrodes showed electrocatalytic activity for non-enzymatic oxidation of glucose at around 0.56V, while no activity or lower results were found on the Ti and the Cu/Ti or the Ni/Ti electrodes respectively.

In addition, the manufactured sensor showed good selectivity for glucose detection in the presence of common interfering molecules. Its applicability was also evaluated in biological samples such as human saliva and urine.
The high electrocatalytic activity of Ni-Cu/Ti was attributed to the synergistic and electronic effect resulting from the combination of Ni and Cu to form a bimetallic Ni-Cu catalyst.
The performance of the as prepared Ni-Cu/Ti allows this material to be considered as a suitable alternate for non-enzymatic electrochemical glucose sensors.

Acknowledgement

The authors would like to thank the Algerian Ministry of Higher Education and the University of Bejaia for their materials support.

Also, they would like to thank Madirel laboratory, Aix- Marseille University for their support and the staff of the Multidisciplinary Center for Electron Microscopy and Microanalysis, especially Dr. Andrea Campos from Aix-Marseille University for surface morphology and composition analysis.

Author contributions information

All authors contributed to the study conception and design. Material preparation, data collection and analysis were performed by Katia Hebbache, Nadia Ait Ahmed, Nabila Aliouane and Marielle Eyraud. The first draft of the manuscript was written by Katia Hebbache and all authors commented the previous version of the manuscript. All authors read and approved the final manuscript.
Approval of the version of the manuscript to be published (the names of all authors must be listed):

K. Hebbache, N. Ait Ahmed, N. Aliouane, M. Eyraud

CRediT taxonomy

Katia Hebbache, investigation, experimental design, writing the original Paper.

Nadia Ait Ahmed, Conceptualization, Supervision and writing-Review

Nabila Aliouane, Supervision-Review

Marielle Eyraud, Supervision, Conceptualization and Review

Data availability

The datasets generated during and/or analyzed during the current study are available from the corresponding author on reasonable request.

Funding interests

No funding was received for conducting this study

Declarations

Competing interests / conflicts of interest

Not applicable, the authors declare no competing and no conflicts interests regarding this paper.

Financial interests

The authors have no relevant financial or non-financial interests to disclose.

Ethical approval

Not applicable

References

[1] Bahadir EB, Sezginturk MK (2015) Applications of commercial biosensors in clinical, food, environmental, and biothreat/biowarfare analyses. Anal. Biochem 478:107–120. https://doi.org/10.1016/j.ab.2015.03.011

[2] Yuan XH, Wang JH, Xia K (2005) Highly ordered platinum-nanotubule arrays for amperometric glucose sensing. Adv. Funct. Mater 15:803–809. https://doi.org/10.1002/adfm.200400321

[3] Chandrasekaran NI, Matheswaran M (2019) A sensitive and selective non-enzymatic glucose sensor with hollow Ni-AlMn layered triple hydroxide nanocomposites modified Ni foam. Sensors and Actuators: B. Chemical 288:188–194. https://doi.org/10.1016/j.snb.2019.02.102

[4] Wei M, Qiao X, Zhao H, Liang J, Li T, Luo Y, Lu S, Shi X, Lu W, Sun X (2020) Electrochemical non-enzymatic glucose sensors: Recent progress and perspectives. Chem. Commun. 56:14553–14569. https://doi.org/10.1039/D0CC05650B

[5] Hu Q, Qin J, Wang XF, Ran GY, Wang Q, Liu GX, Ma JP, Ge JY, Wang HY (2021) Cu-Based Conductive MOF Grown in situ on Cu Foam as a Highly Selective and Stable Non-Enzymatic Glucose Sensor. Front. Chem. 9:786970. https://doi.org/10.3389/fchem.2021.786970

[6] Pandey A, Tripathi P, Pandey R, Srivatava R, Goswami S (2011) Alternative Therapies Useful in the Management of Diabetes: a Systematic Review. J. Pharm. Bioallied Sci. 3:504–512. https://doi.org/10.4103%2F0975-7406.90103

[7] Naikoo GA, Awan T, Salim H, Arshad F, Hassan IU, Pedram MZ, Ahmed W, Faruck HL, Aljabali AAA, Mishra V, Serrano-Aroca A, Goyal R, Negi P, Birkett M, Nasef MM, Charbe NB, |Bakshi HA, Tambuwala MM (2021) Fourth-generation glucose sensors composed of copper nanostructures for diabetes management: A critical review. Bioeng Transl Med. 7:e10248. https://doi.org/10.1002/btm2.10248

[8] Ma ZZ, Liu B, Jiao H, Xu L (2022) A Non−Enzymatic Electrochemical Sensor of Cu@Co−MOF Composite for Glucose Detection with High Sensitivity and Selectivity. Chemosensors 10:416. https://doi.org/10.1039/D1NJ04480J

[9] Mahmoud A, Echabaane M, Omri K, Boudon J, Saviot L, Millot N, Ben Chaabane R (2021) Cu-Doped ZnO Nanoparticles for Non-Enzymatic Glucose Sensing, Molecules 26:929. https://doi.org/10.3390/molecules26040929

[10] Liu F, Wang P, Zhang Q, Wang Z, Liu Y, Zheng Z, Qin X, Zhang X, Dai Y, Li L, B. Huang (2018) Porous Co_3O_4 nanosheets asa high-performance non-enzymatic sensor for glucose detection.Anal. Bioanal. Chem 410:7663–7670. https://doi.org/10.1007/s00216-018-1380-4

[11] Wang M, Shi M, Meng E, Gong F, Li F (2020) Non-enzymatic glucose sensor based on three-dimensional hierarchical Co_3O_4 nanobooks, Micro & Nano Letters 15:191–195. https://doi.org/10.1049/mnl.2019.0552

[12] Jeong H, Nguyen DM, Lee MS, Kim HG, Ko SC, Kwac LK (2018) N-doped graphene-carbon nanotube hybrid networks attaching with gold nanoparticles for glucose non-enzymatic sensor. Mater. Sci. Eng. C 90:38–45. https://doi.org/10.1016/j.msec.2018.04.039

[13] He G, Wang L (2018) One-step preparation of ultra-thin copper oxide nanowire arrays/copper wire electrode for non-enzymatic glucose sensor. Ionics 24:3167–3175. https://link.springer.com/article/10.1007/s11581-018-2513-7

[14] Liu S, Ay A, Luo Q, Hu X, Białas K, Dutta G, Moschou D, Regoutz A (2022) Oxidation of copper electrodes on flexible polyimide substrates for non-enzymatic glucose sensing. Mater. Res. Express 9:045010. https://doi.org/10.1088/2053-1591/ac656f

[15] Liu S, Zeng W, Guo Q, Li Y (2020) Metal oxide based composite for non-enzymatic glucose sensors, Journal of Materials Science: Materials in Electronics 31:16111–16136. https://link.springer.com/article/10.1007/s10854-020-04239-0

[16] Gupta P, Gupta VK, Huseinov A, Rahm CE, Gazica K, Alvarez NT (2021) Highly sensitive non-enzymatic glucose sensor based on carbon nanotube microelectrode set, Sensors and Actuators: B. Chemical 348:130688. https://doi.org/10.1016/j.snb.2021.130688

[17] Dung NQ, Jung DPH, Kim D (2013) A high-performance nonenzymatic glucose sensor made of CuO–SWCNT nanocomposites. Biosens. Bioelectron 42:280–286. https://doi.org/10.1016/j.bios.2012.10.044

[18] Macdonald IA (2016) A review of recent evidence relating to sugars, insulin resistance and diabetes. Eur. J. Nutr. 55:17–23. https://doi.org/10.1007%2Fs00394-016-1340-8

[19] Gabriel MH, Atkins D, Chisholm L, Noblin A (2018) Adverse events among patients with diabetes and ambulatory practice characteristics: evidence from a nationally representative survey. SAGE Open 8 (2018) 2158244018. http://dx.doi.org/10.1177/2158244018782732

[20] Lozano MG, García YP, Gonzalez JAS, Bañuelos CVO, Escareño MPL, Balagurusamy N (2019) Chapter 40 -Biosensors for Food Quality and Safety Monitoring: Fundamentals and Applications, In Enzymes in Food Biotechnology 691-709 Academic Press. https://doi.org/10.1016/B978-0-12-813280-7.00040-2

[21] Teymourian H, Barfidokht A, Wang J (2020) Electrochemical glucose sensors in diabetes management: an updated review (2010–2020). Chem. Soc. Rev. 49:7671–7709. https://doi.org/10.1039/D0CS00304B

[22] Wu D, Hu D, Chen H, Shi G, Fetahu IS, Wu F, Rabidou K, Fang R, Tan L, Xu S, Liu H, C. Argueta C, Zhang L, Mao F, Yan G, Chen J, Dong Z, Lv R, Xu Y, Wang M, Ye Y, Zhang S, Duquette D, Geng S, Shi YG (2018) Glucose-regulated phosphorylation of TET2 by AMPK reveals a pathway linking diabetes to cancer. Nature 559:637–641. https://doi.org/10.1038/s41586-018-0350-5

[23] Dong M, Hu H, Ding S, Wang C, Li L (2021) Fabrication of $NiMn_2O_4$ nanosheets on reduced graphene oxide for non-enzymatic detection of glucose. Materials Technology. Advanced Performance Materials 36:203-211. http://dx.doi.org/10.1080/10667857.2020.1740861

[24] Arif D, Hussain Z, Sohail M, Liaqat MA, Khan MA, Noor T (2020) A Non-enzymatic Electrochemical Sensor for Glucose Detection Based on Ag@TiO_2@ Metal-Organic Framework (ZIF-67) Nanocomposite. Front. Chem 8 573510. https://doi.org/10.3389/fchem.2020.573510

[25] Dhara K, Mahapatra DR (2018) Electrochemical nonenzymatic sensing of glucose using advanced nanomaterials. Microchimica Acta 185:1-32. https://doi.org/10.1007/s00604-017-2609-1

[26] Lu C, Li Z, Ren L, Su N, Lu D, Liu Z (2019) In Situ Oxidation of Cu_2O Crystal for Electrochemical Detection of Glucose. Sensors 19:2926. https://doi.org/10.3390/s19132926

[27] Toghill KE, Compton RG (2010) Electrochemical non-enzymatic glucose sensors: a perspective and an evaluation. Int. J. Electrochem. Sci. 5 :1246–1301. http://www.electrochemsci.org/papers/vol5/5091246.pdf

[28] Hsiao PH, Chen CY (2019) Insights for realizing ultrasensitive colorimetric detection of glucose based on carbon/silver core/shell nanodots. ACS Appl. Bio Mater 2:2528–2538. https://doi.org/10.1021/acsabm.9b00228

[29] Morikawa M, Kimizuka N, Yoshihara M, Endo T (2002) New Colorimetric Detection of Glucose by Means of Electron-Accepting Indicators: Ligand Substitution of [Fe(acac)3−n(phen)n]n+ Complexes Triggered by Electron Transfer from Glucose Oxidase. Chem.sEur. J 8:5580–5584. https://doi.org/10.1002/1521-3765(20021216)8:24%3C5580::AID-CHEM5580%3E3.0.CO;2-V

[30] Lan D, Li B, Zhang Z (2008) Chemiluminescence flow biosensor for glucose based on gold nanoparticle-enhanced activities of glucose oxidase and horseradish peroxidase. Biosens. Bioelectron 24:934–938. https://doi.org/10.1016/j.bios.2008.07.064

[31] Yang X, Zhou Z, Xiao D, Choi MMF (2006) A fluorescent glucose biosensor based on immobilized glucose oxidase on bamboo inner shell membrane. Biosens. Bioelectron 21:1613–1620. https://doi.org/10.1016/j.bios.2005.08.004

[32] Li J, Li X, Weng R, Qiang T, Wang X (2021) Penfluridol triggers mitochondrialmediated apoptosis and suppresses glycolysis in colorectal cancer cells through down-regulating hexokinase-2. Anat. Rec 304:520–530, https://doi.org/10.1002/ar.24464

[33] Yang D, Afroosheh S, Lee JO, Cho H, Kumar S, Siddique RH, Narasimhan V, Yoon YZ, Zayak AT, Choo H (2018) Glucose sensing using surface-enhanced ramanmode constraining. Anal. Chem 90:14269–14278. https://doi.org/10.1021/acs.analchem.8b03420

[34] Shafer-Peltier KE, Haynes CL, Glucksberg MR, Duyne RPV (2003) Toward a glucose biosensor based on surface-enhanced Raman scattering. J. Am. Chem. Soc 125:588–593. https://doi.org/10.1021/ja028255v

[35] Young LEA, Brizzee CO, Macedo JKA, Murphy RD, Contreras CJ, De Paoli-Roach AA, Roach PJ, Gentry MS, Sun RC (2020) Accurate and sensitive quantitation of glucose and glucose phosphates derived from storage carbohydrates by mass spectrometry. Carbohydr. Polym 230:115651. https://doi.org/10.1016/j.carbpol.2019.115651

[36] Wang H, Hu L, Zhou P, Ouyang L, Chen B, Li Y, Chen Y, Zhang Y, Zhou J (2021) Simultaneous determination of fructose, glucose and sucrose by solid phase extraction-liquid chromatography-tandem mass spectrometry and its application to source and adulteration analysis of sucrose in tea. J. Food Compos. Anal 96:103730. https://doi.org/10.1016/j.jfca.2020.103730

[37] Du P, Zhou B, Cai C (2008) Development of an amperometric biosensor for glucose based on electrocatalytic reduction of hydrogen peroxide at the single-walled carbon nanotube/nile blue A nanocomposite modified electrode. Journal of Electroanalytical Chemistry 614:149–156. https://doi.org/10.1016/j.jelechem.2007.11.036

[38] Kandimalla VB, Tripathi VS, Ju H (2006) A conductive ormosil encapsulated with ferrocene conjugate and multiwall carbon nanotubes for biosensing application Biomaterials 27:1167–1174. https://doi.org/10.1016/j.biomaterials.2005.07.018

[39] Xian Y, Hu Y, Liu F, Xian Y, Feng L, Jin L (2007) Template synthesis of highly ordered Prussian blue array and its application to the glucose biosensing. Biosensors and Bioelectronics 22:2827-2833. https://doi.org/10.1016/j.bios.2006.11.020

[40] Wang Z, Liu S, Wu P, Cai C (2009) Detection of Glucose Based on Direct Electron Transfer Reaction of Glucose Oxidase Immobilized on Highly Ordered Polyaniline Nanotubes. Anal. Chem 81:1638–1645. https://doi.org/10.1021/ac802421h

[41] Zhao M, Wu X, Cai C (2009) Polyaniline Nanofibers: Synthesis, Characterization, and Application to Direct Electron Transfer of Glucose Oxidase. J. Phys. Chem. C 113:4987–4996. https://doi.org/10.1021/jp807621y

[42] Rama EC, Costa-García A, Abedul MTF (2017) Pin-based electrochemical glucose sensor with multiplexing possibilities. Biosens. Bioelectron Procedia Technology 88:43–40. http://dx.doi.org/10.1016/j.bios.2016.06.068

[43] Wang J (2001) Glucose biosensors: 40 years of advances and challenges. Electroanalysis 13:983–988. https://doi.org/10.1002/1616-8984(200201)10:1<107::AID-SEUP107>3.0.CO;2-Q

[44] Wang J Electrochemical glucose biosensors (2008) Chem. Rev 108:814–825. https://doi.org/10.1021/cr068123a

[45] Chinnasamy G, Venkatraman P, Sakthivel M, Chen SM, Sangeetha S, Sureka CS (2018) An Efficient and a Highly Sensitive Glucose Sensor Based on CuO Nanodots. SENSOR LETTERS 16:584-589. https://doi.org/10.1166/sl.2018.4004

[46] Liu Q, Lu X, Li J, Yao X, Li J (2007) Direct electrochemistry of glucose oxidase and electrochemical biosensing of glucose on quantum dots/carbon nanotubes electrodes. Biosens. Bioelectron 22:3203–3209. https://doi.org/10.1016/j.bios.2007.02.013

[47] Park S, Boo H, Chung TD (2006) Electrochemical non-enzymatic glucose sensors. Anal. Chim. Acta 556:46–57. https://doi.org/10.1016/j.aca.2005.05.080

[48] Kondepati VR, Heise HM (2007) Recent progress in analytical instrumentation for glycemic control in diabetic and critically ill patients, Anal. Bioanal.Chem 388:545–563. https://doi.org/10.1007/s00216-007-1229-8

[49] Heller A, Feldman B (2008) Electrochemical Glucose Sensors and Their Applications in Diabetes Management. Chemical Reviews 108:2482–505. https://doi.org/10.1021/cr068069y

[50] Wang C, Hu H, Ding S, Dong M, Li L (2022) Highly sensitive electrochemical non-enzymatic glucose biosensor based on squamous $NiCo_2O_4$ nanosheets decorated nitrogen-doped reduced graphene oxide. Materials Technology. Advanced Performance Materials 37:906-914. https://doi.org/10.1080/10667857.2021.1905205

[51] Bairagi PK, Verma N (2019) Electro-polymerized polyacrylamide nano film grown on a Ni-reduced graphene oxide- polymer composite: a highly selective non-enzymatic electrochemical recognition element for glucose. Sensors & Actuators: B. Chemical 289:216–225. https://doi.org/10.1016/j.snb.2019.03.057

[52] Zhou J, Yin H, Wang L, Zhao H, Zhang Z, Gong J, Zheng Y, Nie Q (2021) Electrodeposition of bimetallic NiPt nanosheet arrays on carbon papers for high performance nonenzymatic disposable glucose sensors. J Mater Sci: Mater Electron 32:22493–22505. https://doi.org/10.1007/s10854-021-06735-3

[53] Sehit E, Altintas Z (2020) Significance of nanomaterials in electrochemical glucose sensors: an updated review (2016–2020). Biosens. Bioelectron 159:112165. https://doi.org/10.1016/j.bios.2020.112165

[54] Chen C, Xie Q, Yang D, Xiao H, Fu Y, Tan Y, Yao S (2013) Recent advances in electrochemical glucose biosensors: a review. RSC Adv 3:4473–4491. https://doi.org/10.1039/C2RA22351A

[55] Sun J, Zhao H, Wang Z (2022) Nonenzymatic Glucose Sensor Based on Porous Co_3O_4 Nanoneedles, Hindawi Journal of Environmental and Public Health Volume 2022, Article ID 6442241, 7 pages, https://doi.org/10.1155/2022/6442241

[56] Dong Q, Ryu H, Lei Y (2021) Metal oxide based nonenzymatic electrochemical sensors for glucose detection. Elctrochimica Acta 370:137744. https://doi.org/10.1016/j.electacta.2021.137744

[57] Hoss U, Jeddi I, Schulz M, Budiman E, Bhogal C, McGarraugh G (2010) Continuous glucose monitoring in subcutaneous tissue using factory-calibrated sensors: a pilot study. Diabetes Technol. Therapeutics 12:591–597. https://doi.org/10.1089/dia.2010.0051

[58] Hwang DW, Lee S, Seo M, Chung TD (2018) Recent advances in electrochemical non-enzymatic glucose sensors – A review. Analytica Chimica Acta 1033:1-34. https://doi.org/10.1016/j.aca.2018.05.051

[59] Chu D, Wang Y, Li D, Chu XQ, Ge D, Chen X (2022) Prism-like bimetallic (Ni–Co) alkaline carboxylatebased non-enzymatic sensor capable of exceptionally high catalytic activity towards glucose. Dalton Transactions. The Royal Society of Chemistry 51:15354-15360. https://doi.org/10.1039/D2DT02424A

[60] Lee WC, Kim KB, Gurudatt NG, Hussain KK, Choi CS, Park DS, Shim YB (2019) Comparison of enzymatic and non-enzymatic glucose sensors based on hierarchical Au-Ni alloy with conductive polymer. Biosens. Bioelectron 130:48-54. https://doi.org/10.1016/j.bios.2019.01.028

[61] Wang X, Xia X, Zhang X, Meng W, Yuan C, Guo M (2017) Nonenzymatic glucose sensor based on Ag&Pt hollow nanoparticles supported on TiO_2 nanotubes. Mater. Sci. Eng C 80:174-179. https://doi.org/10.1016/j.msec.2017.05.137

[62] Tang L, Huan K, Deng D, Han L, Zeng Z, Luo L (2020) Glucose sensor based on Pd nanosheets deposited on Cu/Cu_2O nanocomposites by galvanic replacement. Colloids Surf. B Biointerfaces 188:110797. https://doi.org/10.1016/j.colsurfb.2020.110797

[63] Waqas M, Lan J, Zhang X, Fan Y, Zhang P, Liu C, Jiang Z, Wang X, Zeng J, Chen W (2020) Fabrication of non-enzymatic electrochemical glucose sensor based on Pd- Mn alloy nanoparticles supported on reduced graphene oxide. Electroanalysis 32:1226-1236. https://doi.org/10.1002/elan.201900705

[64] Hoa LT, Sun KG, Hur SH (2015) Highly sensitive non-enzymatic glucose sensor based on Pt nanoparticle decorated graphene oxide hydrogel. Sensors Actuators. B Chem 210:618-623. https://doi.org/10.1016/j.snb.2015.01.020

[65] Shen N, Xu H, Zhao W, Zhao Y, Zhang X (2019) Highly responsive and ultra-sensitive non-enzymatic electrochemical glucose sensor based on Au foam. Sensors 19:1203. https://doi.org/10.3390/s19051203

[66] Lee SJ, Lee YJ, Park JY (2013) A micro-fabricated non-enzymaticurine glucose sensor using Nafion coated nanoporous Pt compositeelectrodes. In Sensors IEEE 1–4. https://doi.org/10.1109/ICSENS.2013.6688313

[67] Ma D, X. Tang, Guo M, Lu H, Xu X (2015) Fabrication and characterizationof non enzymatic glucose sensor based on bimetallic hollow Ag/Pt nanoparticles prepared by galvanic replacement reaction. Ionics 21:1417–1426. https://doi.org/10.1007/s11581-014-1290-1

[68] Abunahla H, Mohammad B, Alazzam A, Jaoude MA, Al-Qutayri M, Hadi SA, Al-Sarawi SF (2019) MOMSense: metal-oxide-metal elementary glucose sensor. Sci. Rep 9 :5524. https://doi.org/10.1038/s41598-019-41892-w

[69] Ye JS, Chen CW, Lee CL (2015) Pd nano cube as non-enzymaticglucose sensor, Sens. Actuators B. Chem 208:569–574. https://doi.org/10.1016/j.snb.2014.11.091

[70] Luo J, Jiang S, Zhang H, Jiang J, Liu X (2012) A novel non-enzymatic glucose sensor based on Cu nanoparticle modified graphene sheets electrode, Anal. Chim. Acta 709:47-53. https://doi.org/10.1016/j.aca.2011.10.025

[71] Khosroshahi Z, Karimzadeh F, Kharaziha M, Allafchian A (2020) A non-enzymatic sensor based on three-dimensional graphene foam decorated with Cu-xCu_2O nanoparticles for electrochemical detection of glucose and its application in human serum. Mater. Sci. Eng. C 108:110216. https://doi.org/10.1016/j.msec.2019.110216

[72] Fang L, Cai Y, Huang B, Cao Q, Zhu Q, Tu T, Ye X, Liang B (2021) A highly sensitive nonenzymatic glucose sensor based on Cu/Cu_2O composite nanoparticles decorated single carbon fiber. Journal of Electroanalytical Chemistry 880:114888. https://doi.org/10.1016/j.jelechem.2020.114888

[73] Niu X, Li X, Pan J, He Y, Qiu F, Yan Y (2016) Recent advances in non-enzymatic electrochemical glucose sensors based on non-precious transition metal materials: opportunities and challenges. RSC Adv. 6 :84893-84905. https://doi.org/10.1039/C6RA12506A

[74] Zhang L, Y. Ding Y, Li R, Ye C, Zhaoa G, Wang Y (2017) Ni-based metal-organic frameworkderived Ni@C nanosheets on a Ni foam substrate as a supersensitivenon-enzymatic glucose sensor. J. Mater. Chem. B 5:5549–5555. https://doi.org/10.1039/C7TB01363A

[75] Babitha KB, Soorya PS, Mohamed AP, Rakhi RB, Ananthakumar S (2020) Development of ZnO@rGO nanocomposites for the enzyme free electrochemical detection of urea and glucose. Mater. Adv 1:1939-1951. https://doi.org/10.1039/D0MA00445F

[76] Hovancov´ J, Šišoláková I, Vanýsek P, Oriňaková R, Shepa I, Kaňuchová M, Király N, Vojtko M, Čudek P, OriňakA (2020) Ligand-to-metal charge transfer (LMCT) complex: new approach to non-enzymatic glucose sensors based on TiO_2, J. Electroanal. Chem 878:114589. https://doi.org/10.1016/j.jelechem.2020.114589

[77] Zhu H, Li L, Zhou W, Shao Z, Chen X (2016) Advances in non-enzymatic glucose sensors based on metal oxides. J. Mater. Chem B 4:7333-7349. https://doi.org/10.1039/C6TB02037B

[78] Zhang L, Yang C, Zhao G, Mu J, Wang Y (2015) Self-supported porous CoOOH nanosheet arrays as a non-enzymatic glucose sensor with good repro-ducibility'. Sens. Actuators B. Chem 210:190–196. https://doi.org/10.1016/j.snb.2014.12.113

[79] Yang J, Cho M, Pang C, Lee Y (2015) Highly sensitive non-enzymatic glucose sensor based on over-oxidized polypyrrole nanowire smodified with $Ni(OH)_2$ nanoflakes. Sens. Actuators B. Chem 211:93–101. https://doi.org/10.1016/j.snb.2015.01.045

[80] Mai HH, Tran DH, Janssens E (2019) Non-enzymaticfluorescentglucose sensor using vertically aligned ZnO nanotubes grown by aone-step. seedless hydrothermal method. Microchim. Acta 186:1-10. https://doi.org/10.1007/s00604-019-3353-5

[81] Wu X, Bao C, Niu Q, Lu W (2019) A novel method to construct a3D $FeWO_4$ microsphere-array electrode as a non-enzymatic glucosesensor. Nanotechnology 30:165501. 10.1088/1361-6528/aafe53

[82] Song MJ (2018) Non-enzymatic glucose sensor based on a copper oxide nanoflowers electrode decorated with Pt nanoparticles. Korean Chem. Eng. Res 56:705–710. https://doi.org/10.9713/kcer.2018.56.5.705

[83] Zhang A, Tian Y, Liu M, Xiao Y, Jia D, Li F (2014) Enhanced performances of nonenzymatic glucose sensors by attaching Au nanoparticles on to the surfaces of Cu-$_2$O@Cu nanocable arrays. RSC Adv 4:43973–43976. https://doi.org/10.1039/C4RA07270G

[84] Li X, Sun Y, Zhang X, Guo J (2018) Co_3O_4 nanosheets anchored on SiO_2 nanospheres for non-enzymatic glucose sensor. J. Nanosci. Nanotechnol18:7251–7254. https://doi.org/10.1166/jnn.2018.15450

[85] Khun K, Ibupoto ZH, Liu X, Beni V, Willander M (2015) The ethylene glycol template assisted hydrothermal synthesis of Co3O4 nanowires; structural char-acterization and their application as glucose non-enzymatic sensor. Mater. Sci. Eng : B 194 :94–100. https://doi.org/10.1016/j.mseb.2015.01.001

[86] Gao Z, Zhang L, Ma C, Zhou Q, Tang Y, Tu Z, Yang W, Cui L, Li Y (2016) TiO_2 decorated Co_3O_4 acicular nanotube arrays and its application as a non-enzymatic glucose sensor. Biosensors and Bioelectronics 80:511–518. https://doi.org/10.1016/j.bios.2016.02.004

[87] Mahmoudian MR, Basirun WJ, Woi PM, Sookhakian M, Yousefi R, Ghadimi H, Alias Y (2016) Synthesis andcharacterization of Co_3O_4 ultra-nanosheets and Co_3O_4 ultra-nanosheet-$Ni(OH)_2$ as non-enzymatic electrochemical sensors for glucose detection. Mater. Sci. Eng: C 59:500–508. https://doi.org/10.1016/j.msec.2015.10.055

[88] Tian L, He G, Cai Y, Wu S, Su Y, Yan H, Yang C, Chen Y, Li L (2018) Co_3O_4 based non-enzymatic glucose sensor with high sensitivity and reliable stability derived from hollow hierarchical architecture. Nanotechnology 29:075502. 10.1088/1361-6528/aaa1d2

[89] Abuzaied MM, Asal YM, Mohammad AM, Al-Akraa IM (2020) Enhanced Glucose Electrooxidation at Ni-Cu Binary Oxide Nanocatalyst, Int. J. Electrochem. Sci 15:2449–2457. https://doi.org/10.20964/2020.03.57

[90] Bai Y, Sun YY, Sun CQ (2008) Pt-Pb nanowire array electrode for enzyme-free glucose detection. Biosensors and Bioelectronics 24:579–585. https://doi.org/10.1016/j.bios.2008.06.003

[91] Ryu J, Kim K, Kim HS, Hahn HT, Lashmore D (2010) Intense pulsed light induced platinum-gold alloy formation on carbon nanotubes for non-enzymatic glucose detection. Biosensors and Bioelectronics 26:602–607. https://doi.org/10.1016/j.bios.2010.07.021

[92] Noh HB, Lee KS, Chandra P, Won MS, Shim YB (2012) Application of a Cu–Co alloy dendrite on glucose and hydrogen peroxide sensors. Electrochimica Acta 61:36–43. https://doi.org/10.1016/j.electacta.2011.11.066

[93] Mahshid SS, Mahshid S, Dolati A, M. Ghorbani M, Yang LX, Luo SL, Cai QY (2011) Template-based electrodeposition of Pt/Ni nanowires and its catalytic activity towards glucose oxidation. Electrochimica Acta 58:551–555. https://doi.org/10.1016/j.electacta.2011.09.083

[94] Nisar S, Tariq M, Muhammad S, Saqib M, Akbar F (2020) Electrocatalytic efficacy of Ni-Cu@VC-72: Non-enzymatic electrochemical detection of glucose using Ni-Cu nanoparticles loaded on carbon black. Synthetic Metals 269:116578. https://doi.org/10.1016/j.synthmet.2020.116578

[95] Lim JE, Ahn SH, Jang JH, Park H, Kim SK (201) Electrodeposited Ni-Cu Alloy Catalysts for Glucose Oxidation. Bull. Korean Chem. Soc 35:2019-2024. http://dx.doi.org/10.5012/bkcs.2014.35.7.2019

[96] Jafarian M, Forouzandeh F, Danaee I, Gobal F, Mahjani M (2009) Electrocatalytic oxidation of glucose on Ni and NiCu alloy modified glassy carbon electrode. J Solid State Electrochem 13:1171–1179. https://doi.org/10.1007/s10008-008-0632-1

[97] Marioli JM, Luo PF, Kuwana T (1993) Nickel-chromium alloy electrode as a carbohydrate detector for liquid chromatography. Analytica Chimica Acta 282:571-580. https://doi.org/10.1016/0003-2670(93)80122-2

[98] J. M. Marioli, T. Kuwana (1993) Electrochemical Detection of Carbohydrates at Nickel Copper and Nickel-Chromium-Iron Alloy Electrodes. Electroanalysis 5:11-15. https://doi.org/10.1002/elan.1140050104

[99] Khulbe KC, Mann RS, Manoogian A (1980) Behavior of Nickel-Copper Alloy in Hydrogenatlon, Orthohydrogen-Parahydrogen Conversion, and H_2-D_2. Exchange Reaction. Chemical Reviews 80:417-428. https://doi.org/10.1021/cr60327a003

[100] Chang JK, Hsu SH, Sun IW, Tsai WT (2008) Formation of nanoporous nickel by selective anodic etching of the nobler copper component from electrodeposited nickel− copper alloys. J. Phys. Chem. C 112:1371–1376. https://doi.org/10.1021/jp0772474

[101] Oriňáková R, Turoňová A, Kladeková D, Gálová M, Smith RM (2006) Recent developments in the electrodeposition of nickel and some nickel-based alloys. J. Appl. Electrochem; 36:957-972. https://doi.org/10.1007/s10800-006-9162-7

[102] Albatat R, Gomez E, Muller C, Sarret M, Vallés E (1991) Electrochemical nucleation of nickel on vitreous carbon electrodes: the influence of organic additives. J. Appl. Electrochem 21:709-715. https://doi.org/10.1007/BF01034050

[103] Khelladi MR, Mentar L, Azizi A, Sahari A, Kahoul A (2009) Electrochemical nucleation and growth of copper deposition onto FTO and n-Si (1 0 0) electrodes. Mater Chem Phys 115:385-390. https://doi.org/10.1016/j.matchemphys.2008.12.017

[104] Wanga S, Guoa X, Yanga H, Dai J, Zhua R, Gonga J, Penga L, Ding W (2014) Electrodeposition mechanism and characterization of Ni–Cu alloy coatings from a eutectic-based ionic liquid. Applied Surface Science 288:530–536. https://doi.org/10.1016/j.apsusc.2013.10.065

[105] Varea A, Pellicer E, Pané S, Nelson BJ, Suriñach S, Baró MD, Sort J (2012) Mechanical Properties and Corrosion Behaviour of Nanostructured Cu-rich CuNi Electrodeposited Films. Int. J. Electrochem. Sci 7:1288 – 1302. http://www.electrochemsci.org/

[106]: Brenner A (1963) Electrodeposition of Alloys. Academic Press, New York/London 1: 40

[107] Sarac U, Baykul MC (2013) Morphological and microstructural properties of two-phase Ni–Cu films electrodeposited at different electrolyte temperatures, Journal of Alloys and Compounds 552:195–201. https://doi.org/10.1016/j.jallcom.2012.10.071

[108]: Yi W, Liu J, Chen H, Gao Y, Li H (2015) Copper/nickel nanoparticle decorated carbon nanotubes for nonenzymatic glucose biosensor. J Solid State Electrochem 19:1511–1521. https://doi.org/10.1007/s10008-015-2766-2

[109] Taherimanesh A, Rashidi AM, Zangeneh S (2020) The Effect of Bath pH and Temperature on the Corrosion Behavior of Co-Electrodeposited Ni-Cu/Cr_2O_3 Nanocomposite Coatings. JMEPEG 29:7863–7871. https://doi.org/10.1007/s11665-020-05301-y

[110] Yang Y, Wang Y, Bao X, Li H (2016) Electrochemical deposition of Ni nanoparticles decorated ZnO hexagonal prisms as an effective platform for non-enzymatic detection of glucose. Journal of Electroanalytical Chemistry 775:163–170. https://doi.org/10.1016/j.jelechem.2016.04.041

[111] Abdel Hameed RM (2013) Amperometric glucose sensor based on nickel nanoparticles/ carbon Vulcan XC-72R. Biosensors and Bioelectronics 47:248–257. https://doi.org/10.1016/j.bios.2013.02.044

[112] Nie H, Yao Z, Zhou X, Yang Z, Huang S (2011) Nonenzymatic electrochemical detection of glucose using well-distributed nickel nanoparticles on straight multi-walled carbon nanotubes, Biosensors and Bioelectronics 30:28–34. https://doi.org/10.1016/j.bios.2011.08.022

[113] Hui N, Wang S, Xie H, Xu S, Niu S, Luo X (2015) Nickel nanoparticles modified conducting polymer composite of reduced graphene oxide doped poly(3,4-ethylenedioxythiophene) for enhanced nonenzymatic

glucose sensing. Sensors and Actuators B: Chemical 221:606-613. https://doi.org/10.1016/j.snb.2015.07.011

[114] Lv X, Tan R, Xu X, Li Y, Geng C, Fang Y, Tan C, Cui B, Wang L (2022) A highly sensitive non-enzymatic glucose sensor based on CuNi nanoalloys through one-step electrodeposition strategy. Journal of Applied Electrochemistry 52:895–905. https://doi.org/10.1007/s10800-022-01671-4

[115] Nacef M, Chelaghmia ML, Affoune AM, Pontie´ M (2019) Electrochemical Investigation of Glucose on a Highly Sensitive Nickel-Copper Modified Pencil Graphite Electrode. Electroanalysis 31:113–120. https://doi.org/10.1002/elan.201800622

[116] Wang J, Bao W, Zhang L (2012) A nonenzymatic glucose sensing platform based on Ni nanowire modified electrode. Anal. Methods 4:4009–4013. https://doi.org/10.1039/C2AY25759A

[117] Qin L, He L, Zhao J, Zhao B, Yin Y, Yang Y (2017) Synthesis of Ni/Au multilayer nanowire arrays for ultrasensitive non-enzymatic sensing of glucose. Sensors and Actuators B: Chemical 240:779–784. https://doi.org/10.1016/j.snb.2016.09.041

[118] Emir G, Dilgin Y, Ramanaviciene A, Ramanavicius A (2021) Amperometric Nonenzymatic Glucose Biosensor based on Graphite Rod Electrode Modified by Ni-Nanoparticle/Polypyrrole Composite. Microchemical Journal 161:105751. https://doi.org/10.1016/j.microc.2020.105751

[119] Gao X, Du X, Liu D, Gao H, Wang P, Yang J (2020) Core-shell gold-nickel nanostructures as highly selective and stable nonenzymatic glucose sensor for fermentation process. Scientific Reports 10:1365. https://doi.org/10.1038/s41598-020-58403-x

[120] Zhu J, Liu S, Hu Z, Zhang X, Yi N,Tang K, Dexheimer MG, Lian X, Wang Q, Yang J, Gray J, Cheng H (2021) Laser-induced graphene non-enzymatic glucose sensors for on-body measurements. Biosensors and Bioelectronics 193:113606. https://doi.org/10.1016/j.bios.2021.113606

[121] Lin KC, Lin YC, Chen SM (2013) A highly sensitive nonenzymatic glucose sensor based on multi-walled carbon nanotubes decorated with nickel and copper nanoparticles. Electrochimica Acta 96:164–172. https://doi.org/10.1016/j.electacta.2013.02.098

[122] Franceschini F, Taurino I (2022) Nickel-based catalysts for non-enzymatic electrochemical sensing of glucose: A review. Physics in Medicine. 14:100054. https://doi.org/10.1016/j.phmed.2022.100054

[123] Balkourani G, Damartzis T, Brouzgou A, Tsiakaras P (2022) Cost Effective Synthesis of Graphene Nanomaterials for Non-Enzymatic Electrochemical Sensors for Glucose: A Comprehensive Review**.** Sensors 22:355. https://doi.org/10.3390/s22010355

[124] Shabbir SA, Shamaila S, zafar N, Bokhari A, Sabah A (2018) Nonenzymatic glucose sensor with high performance electrodeposited nickel/copper/carbon nanotubes nanocomposite electrode. Journal of Physics and Chemistry of Solids 120:12–19. https://doi.org/10.1016/j.jpcs.2018.04.015

[125] Barbee B, Muchharla B, Adedeji A, Karoui A, Kumar Sadasivuni K, Sha MS, Kumar B (2022) Cu and Ni Co-sputtered heteroatomic thin film for enhanced nonenzymatic glucose detection. *Scientific Reports*, *12*: 7507. https://doi.org/10.1038/s41598-022-11563-4

[126] Wang Q, Cui X, Chen J, Zheng X, Liu C, Xue T, Wang H, Jin Z, Qiao L, Zheng W (2012) Well-dispersed palladium nanoparticles on graphene oxide as a nonenzymatic glucose sensor. RSC Adv. 2:6245–6249. https://doi.org/ 10.1039/c2ra20425h

[127] Mahmoud A, Echabaane M, Omri K, El Mir L, Ben Chaabane R (2019) Development of an impedimetric non enzymatic sensor based on ZnO and Cu doped ZnO nanoparticles for the detection of glucose. Journal of Alloys and Compounds 786:960e968. https://doi.org/10.1016/j.jallcom.2019.02.060

Figures: Graphics program was used to create the artwork is Origin 6

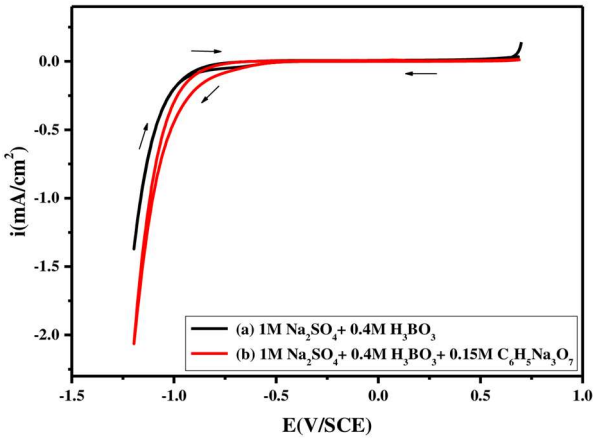

Fig.1

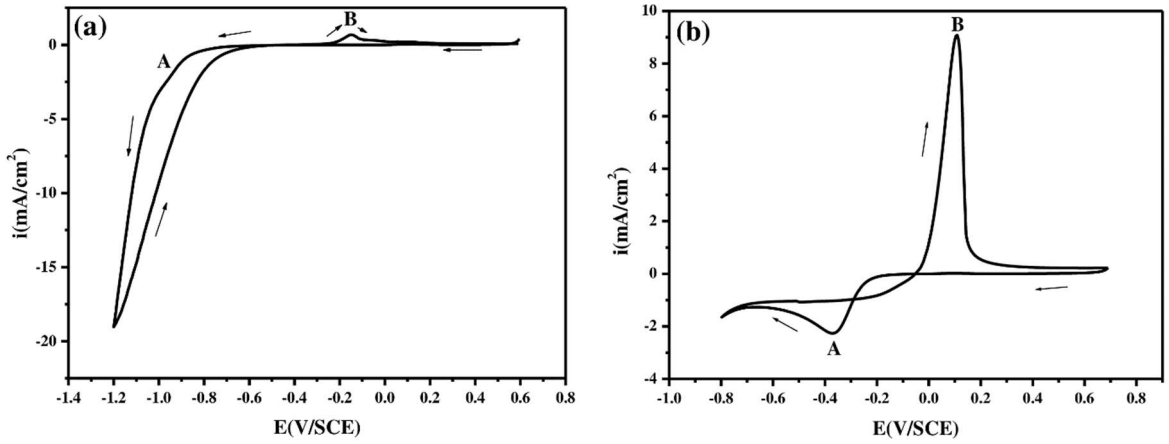

Fig.2

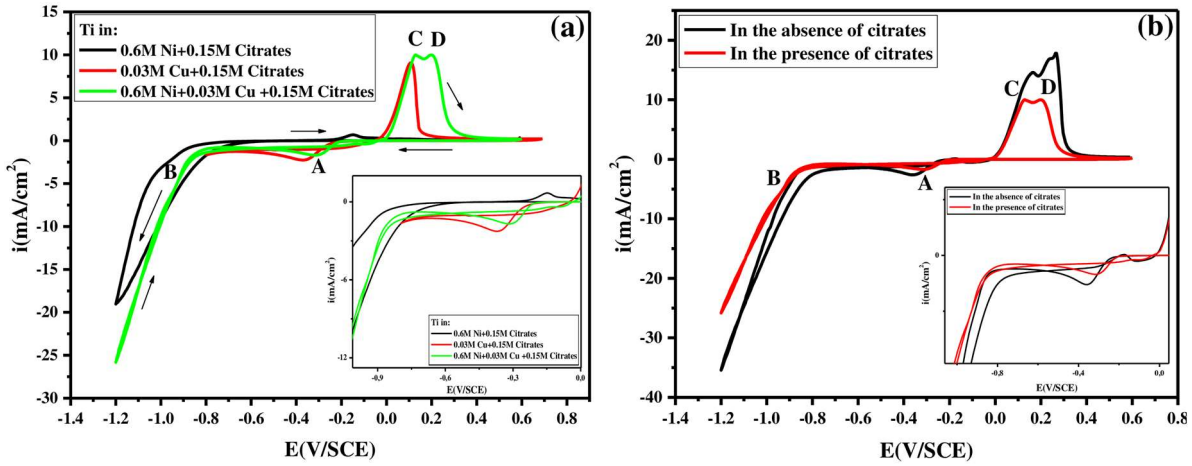

Fig.3

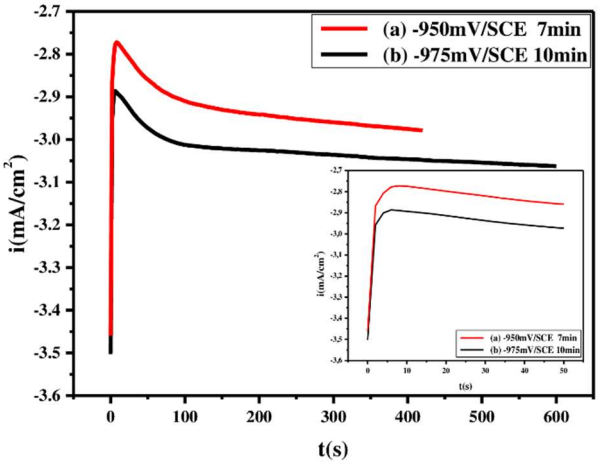

Fig.4

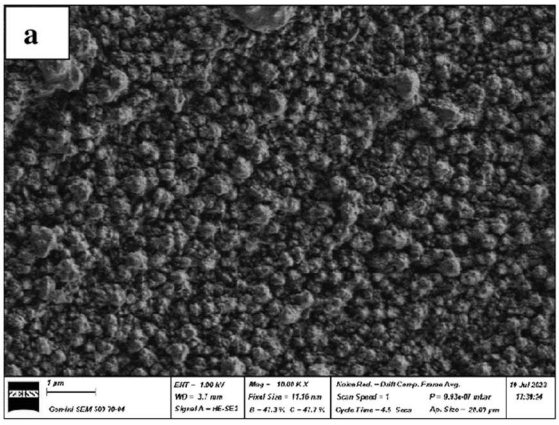

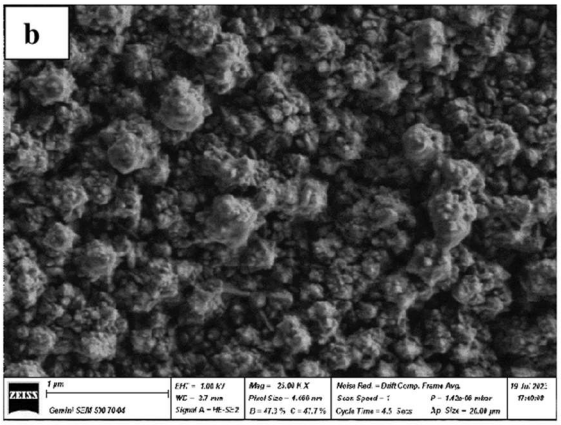

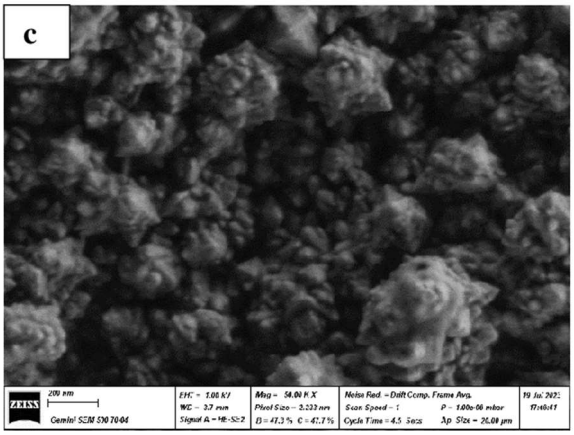

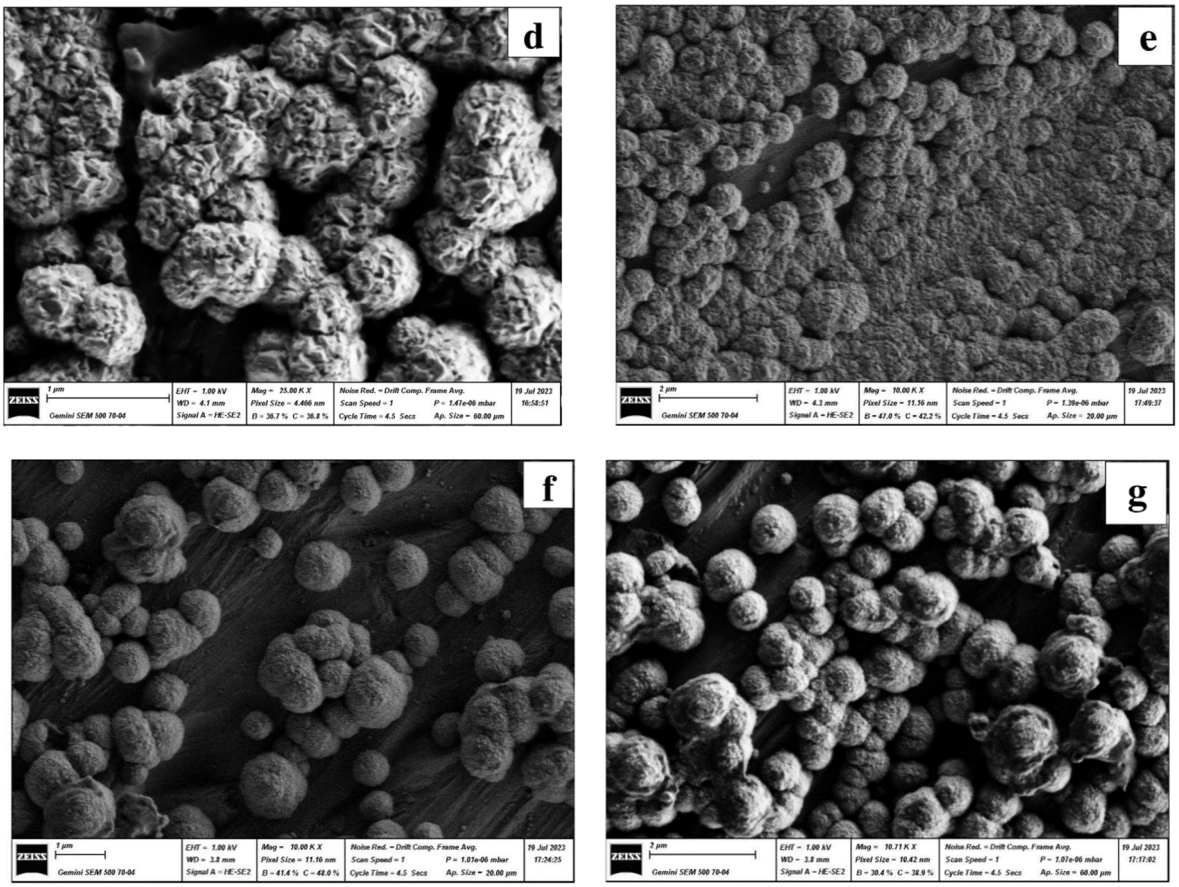

Fig.5

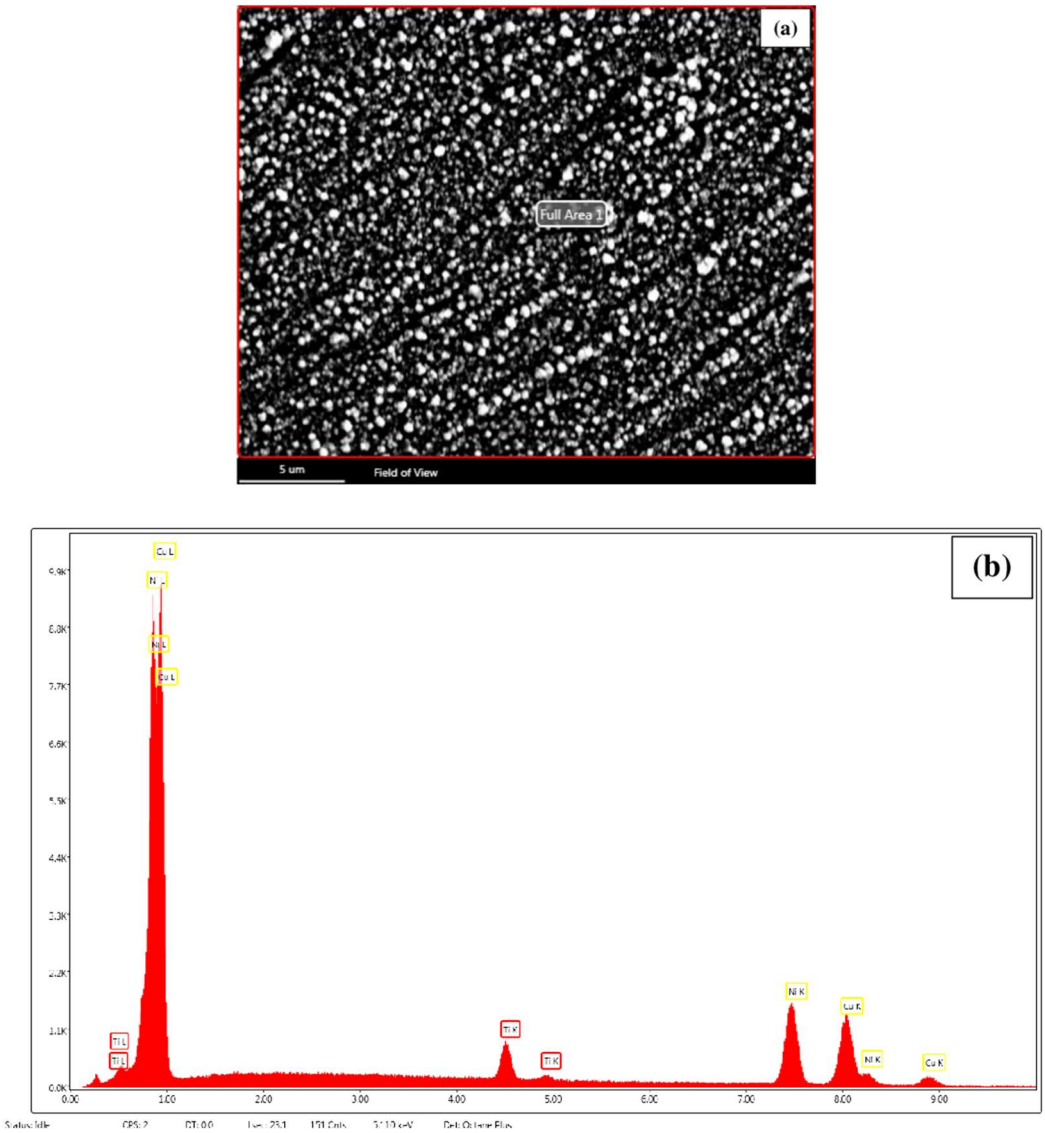
(a)
Full Area 1
5 um
Field of View
(b)
Cu L
Ni L
Ti L
Ti K
Ni K
Cu K
0.00
1.00
2.00
3.00
4.00
5.00
6.00
7.00
8.00
9.00

Fig.6

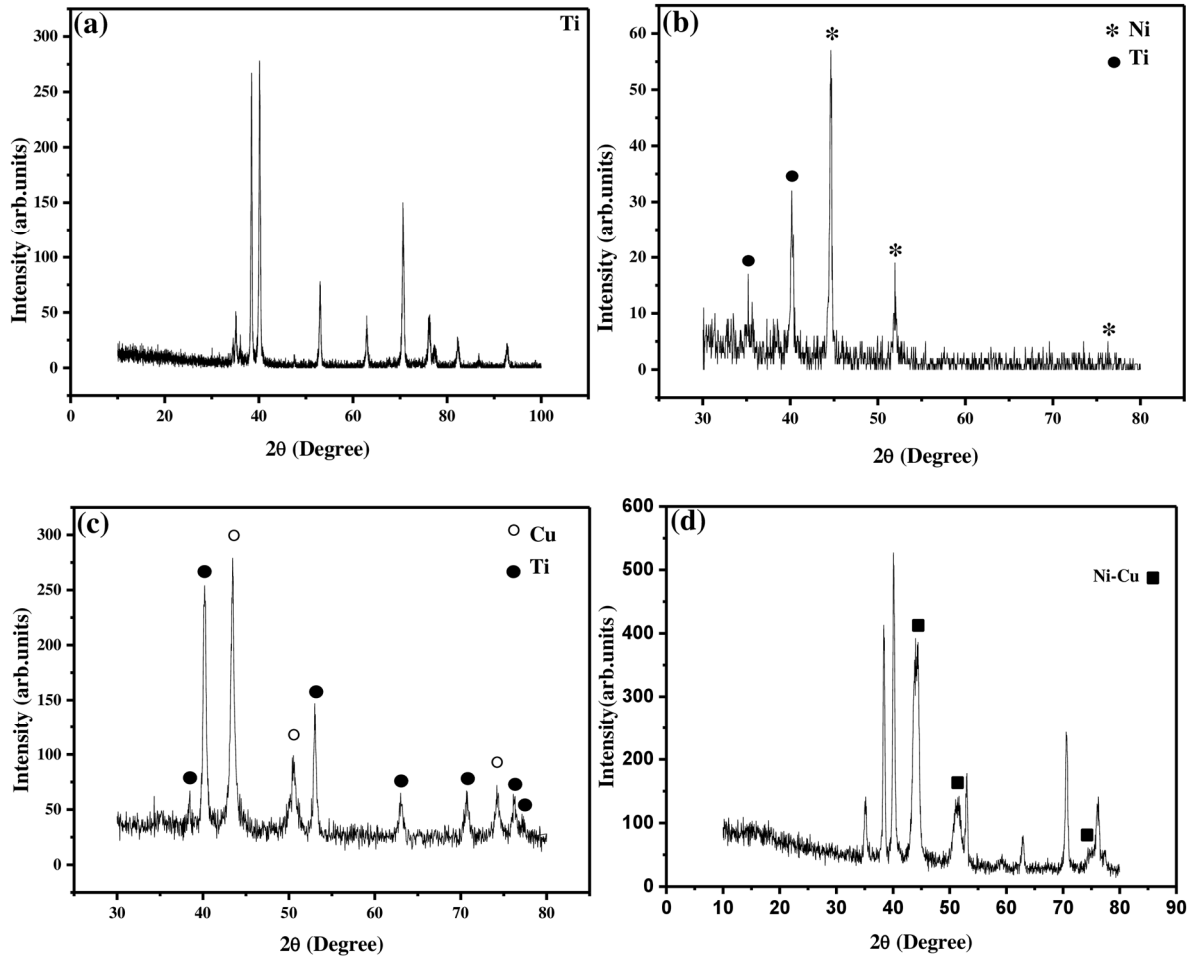
(a)
Ti
Intensity (arb.units)
2θ (Degree)
(b)
* Ni
● Ti
Intensity (arb.units)
2θ (Degree)
(c)
○ Cu
● Ti
Intensity (arb.units)
2θ (Degree)
(d)
Ni-Cu ■
Intensity(arb.units)
2θ (Degree)

Fig.7

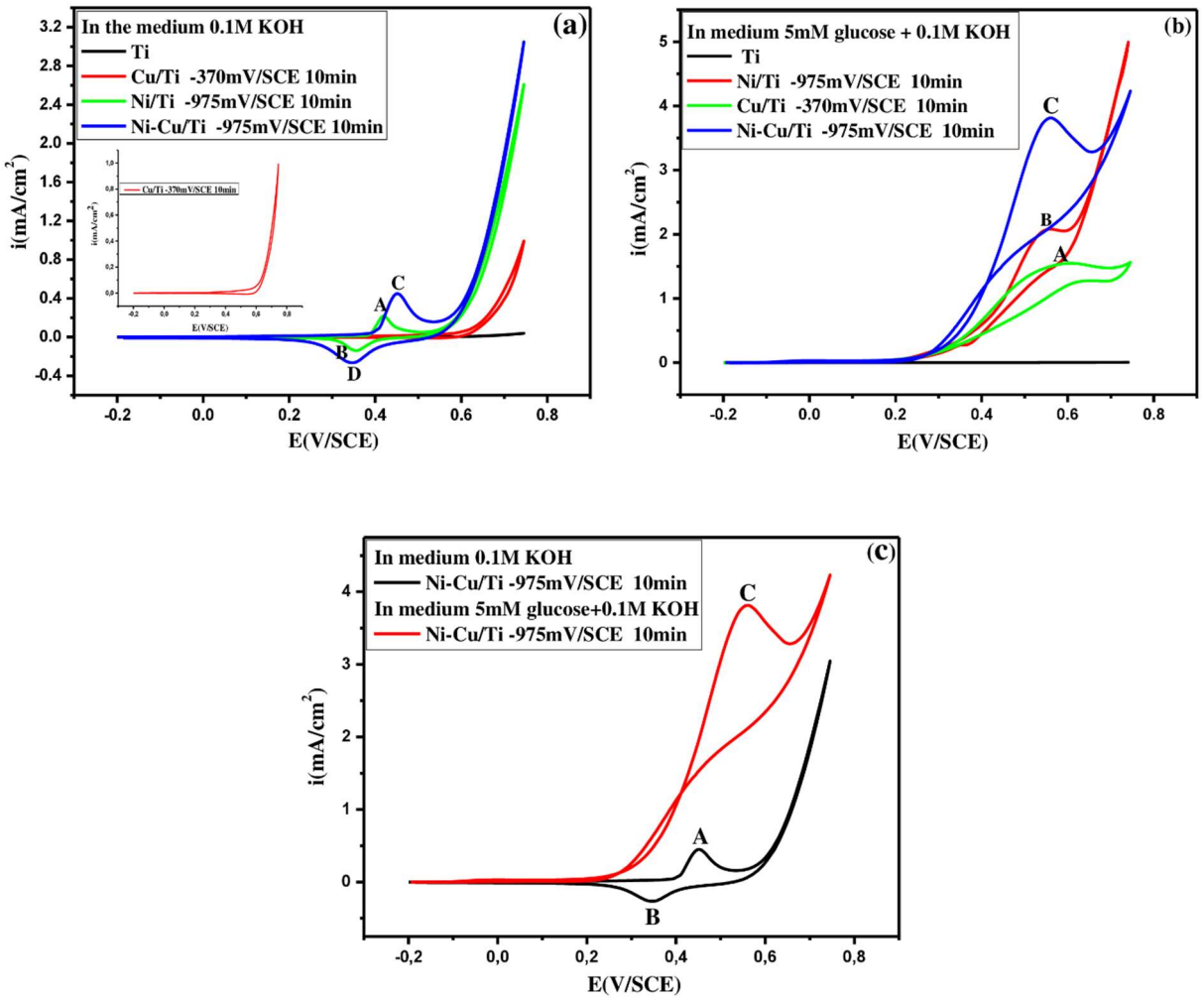
(a)
In the medium 0.1M KOH
Ti
Cu/Ti -370mV/SCE 10min
Ni/Ti -975mV/SCE 10min
Ni-Cu/Ti -975mV/SCE 10min
Cu/Ti -370mV/SCE 10min
E(V/SCE)
A
B
C
D
i(mA/cm2)
E(V/SCE)
(b)
In medium 5mM glucose + 0.1M KOH
Ti
Ni/Ti -975mV/SCE 10min
Cu/Ti -370mV/SCE 10min
Ni-Cu/Ti -975mV/SCE 10min
A
B
C
i(mA/cm2)
E(V/SCE)
(c)
In medium 0.1M KOH
Ni-Cu/Ti -975mV/SCE 10min
In medium 5mM glucose+0.1M KOH
Ni-Cu/Ti -975mV/SCE 10min
A
B
C
i(mA/cm2)
E(V/SCE)

Fig.8

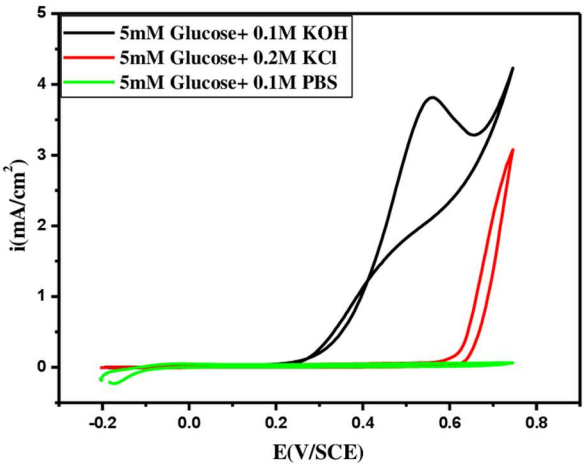
5mM Glucose+ 0.1M KOH
5mM Glucose+ 0.2M KCl
5mM Glucose+ 0.1M PBS
i(mA/cm2)
E(V/SCE)

Fig.9

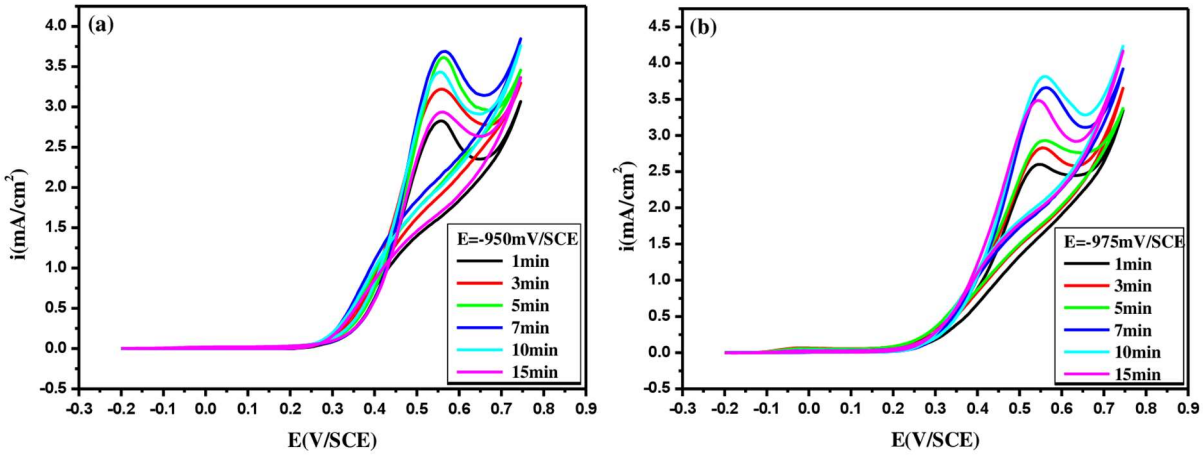
(a)
i(mA/cm^2)
E(V/SCE)
E=-950mV/SCE
1min
3min
5min
7min
10min
15min
(b)
i(mA/cm^2)
E(V/SCE)
E=-975mV/SCE
1min
3min
5min
7min
10min
15min

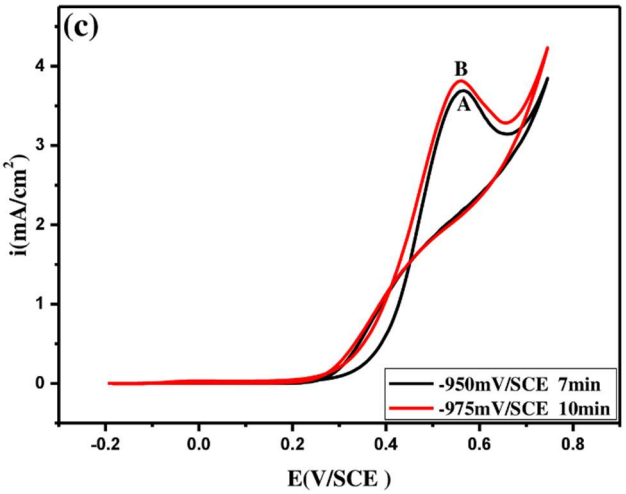
(c)
B
A
i(mA/cm^2)
E(V/SCE)
-950mV/SCE 7min
-975mV/SCE 10min

Fig.10

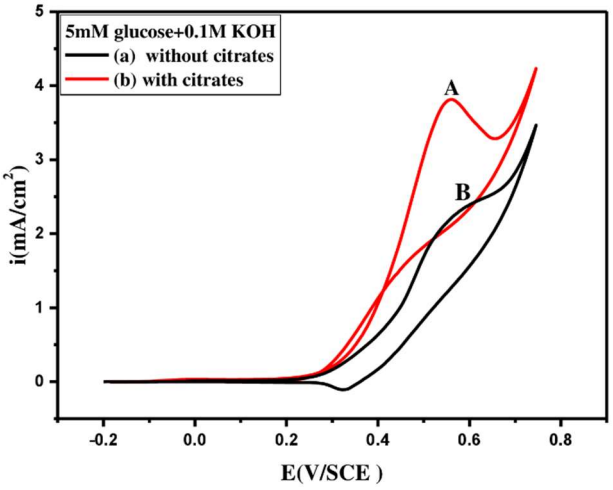
5mM glucose+0.1M KOH
(a) without citrates
(b) with citrates
A
B
i(mA/cm^2)
E(V/SCE)

Fig.11

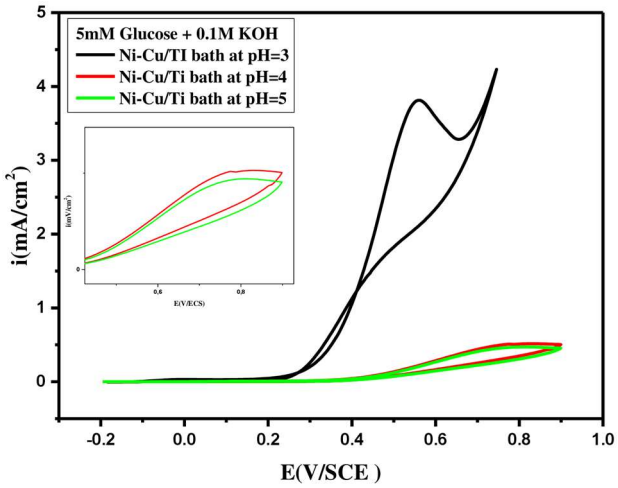

Fig.12

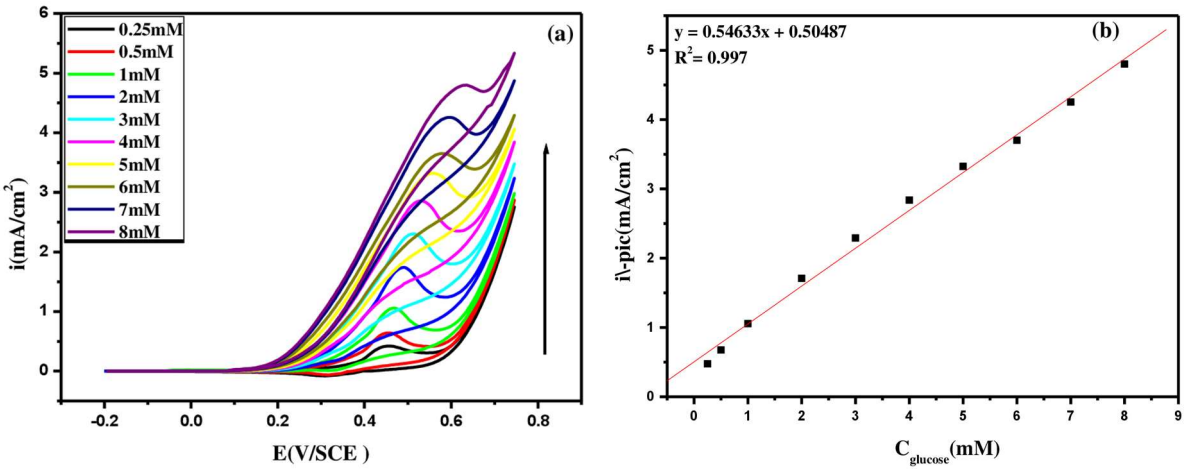

Fig.13

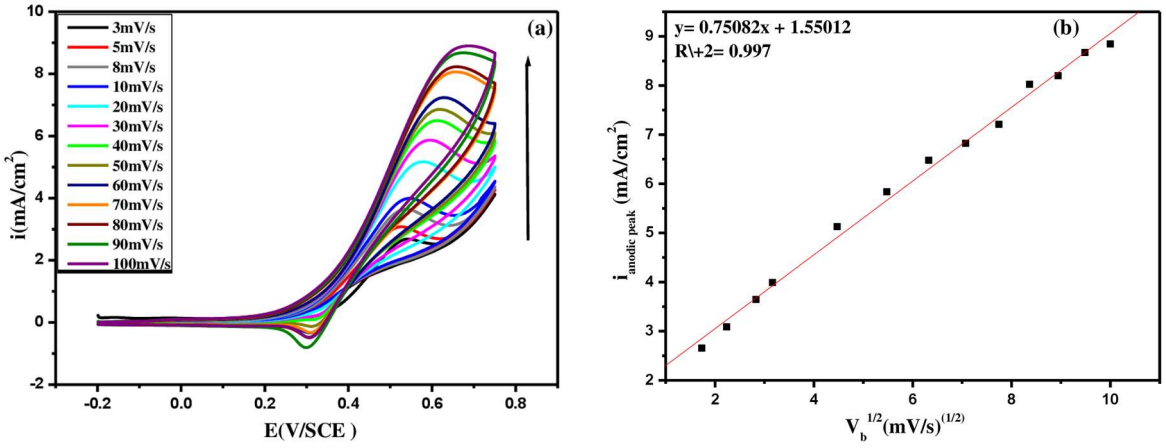

Fig.14

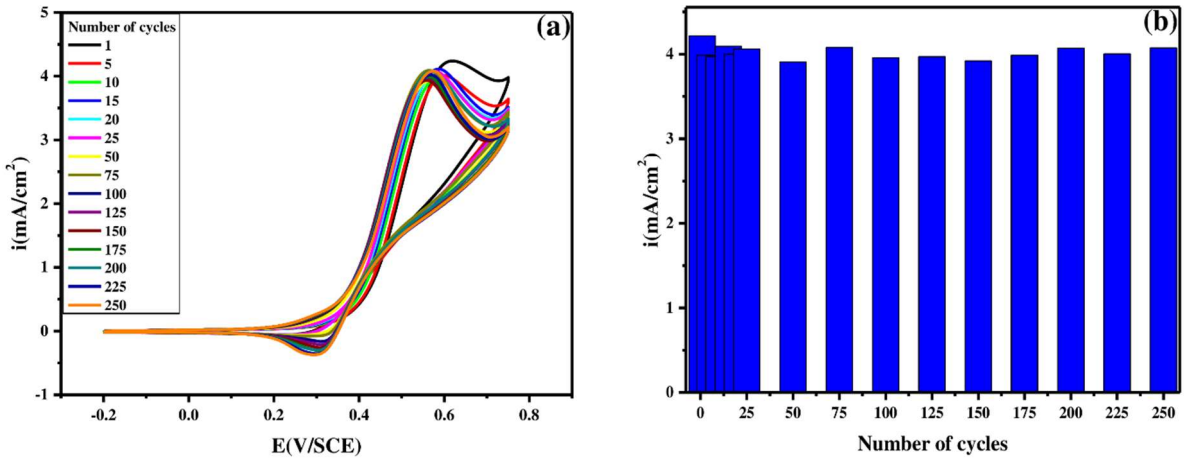
(a)
Number of cycles
1
5
10
15
20
25
50
75
100
125
150
175
200
225
250
i(mA/cm^2)
E(V/SCE)
(b)
i(mA/cm^2)
Number of cycles

Fig. 15

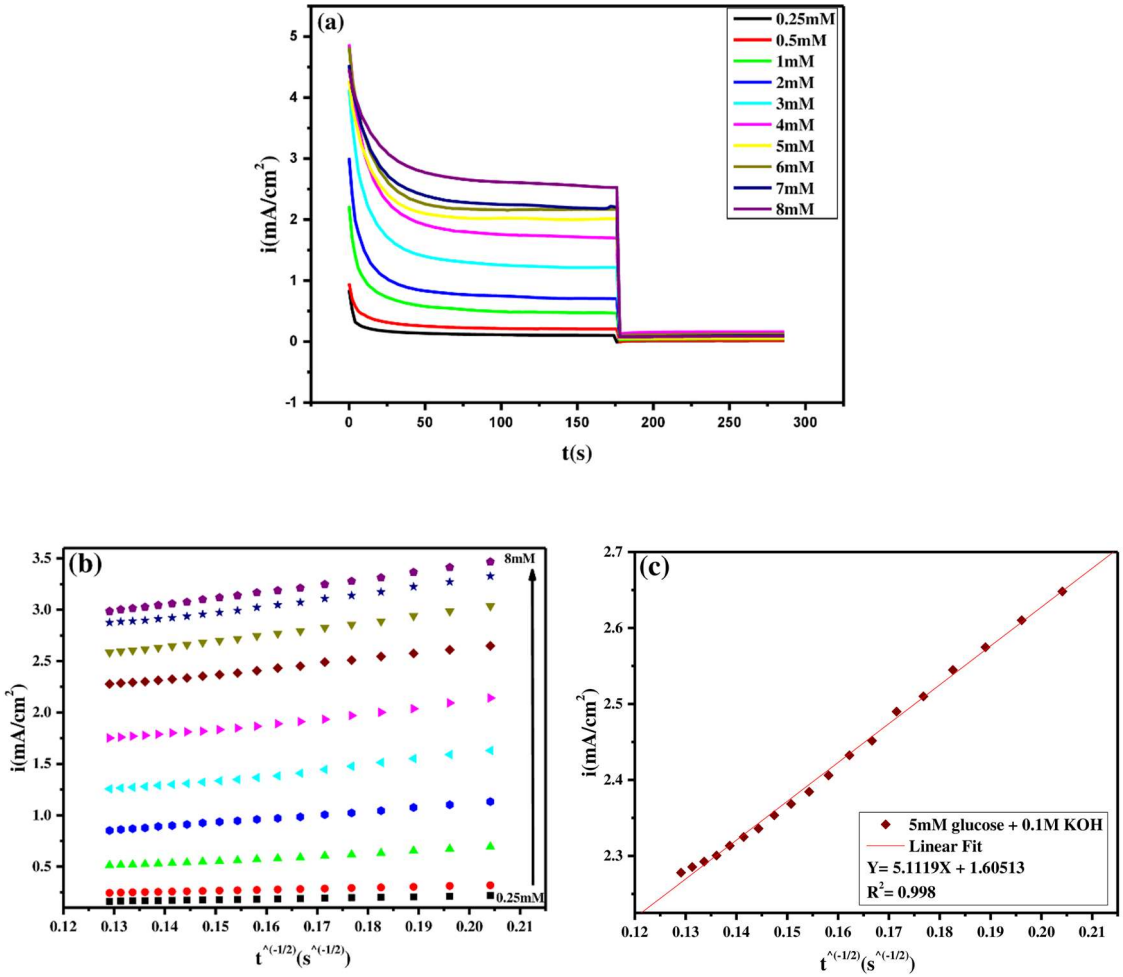
(a)
0.25mM
0.5mM
1mM
2mM
3mM
4mM
5mM
6mM
7mM
8mM
i(mA/cm^2)
t(s)
(b)
8mM
0.25mM
i(mA/cm^2)
t^(-1/2)(s^(-1/2))
(c)
5mM glucose + 0.1M KOH
Linear Fit
Y= 5.1119X + 1.60513
R^2= 0.998
i(mA/cm^2)
t^(-1/2)(s^(-1/2))

Fig.16

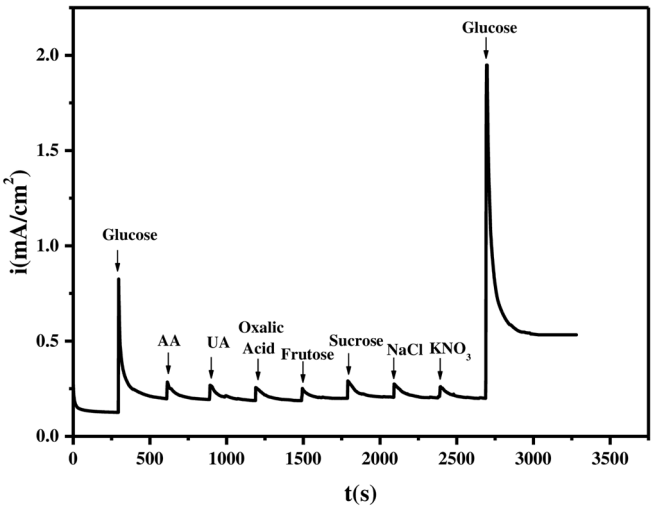
Glucose
Glucose
AA
UA
Oxalic
Acid
Frutose
Sucrose
NaCl
KNO3
i(mA/cm2)
t(s)

Fig.17

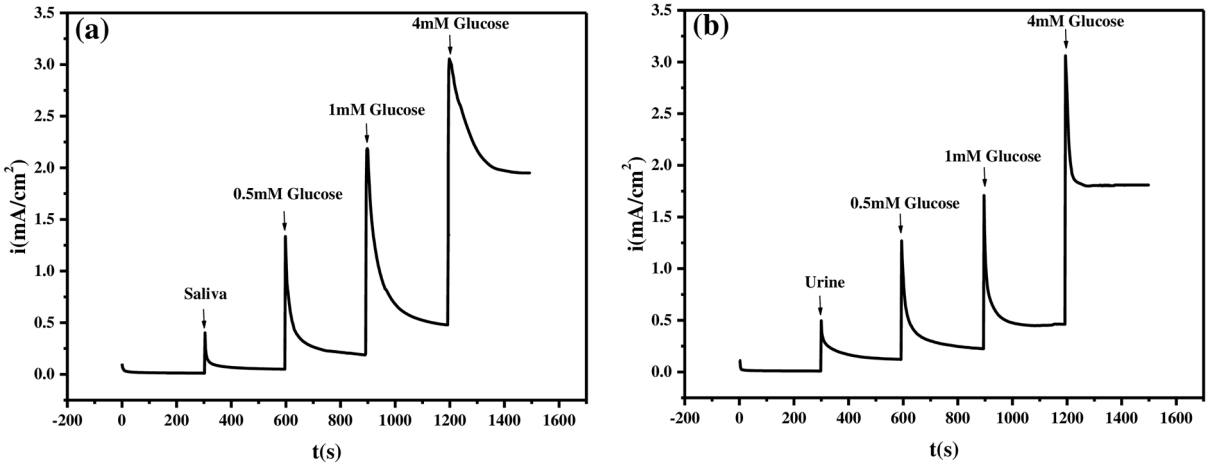
(a)
4mM Glucose
1mM Glucose
0.5mM Glucose
Saliva
i(mA/cm2)
t(s)
(b)
4mM Glucose
1mM Glucose
0.5mM Glucose
Urine
i(mA/cm2)
t(s)

Fig.18

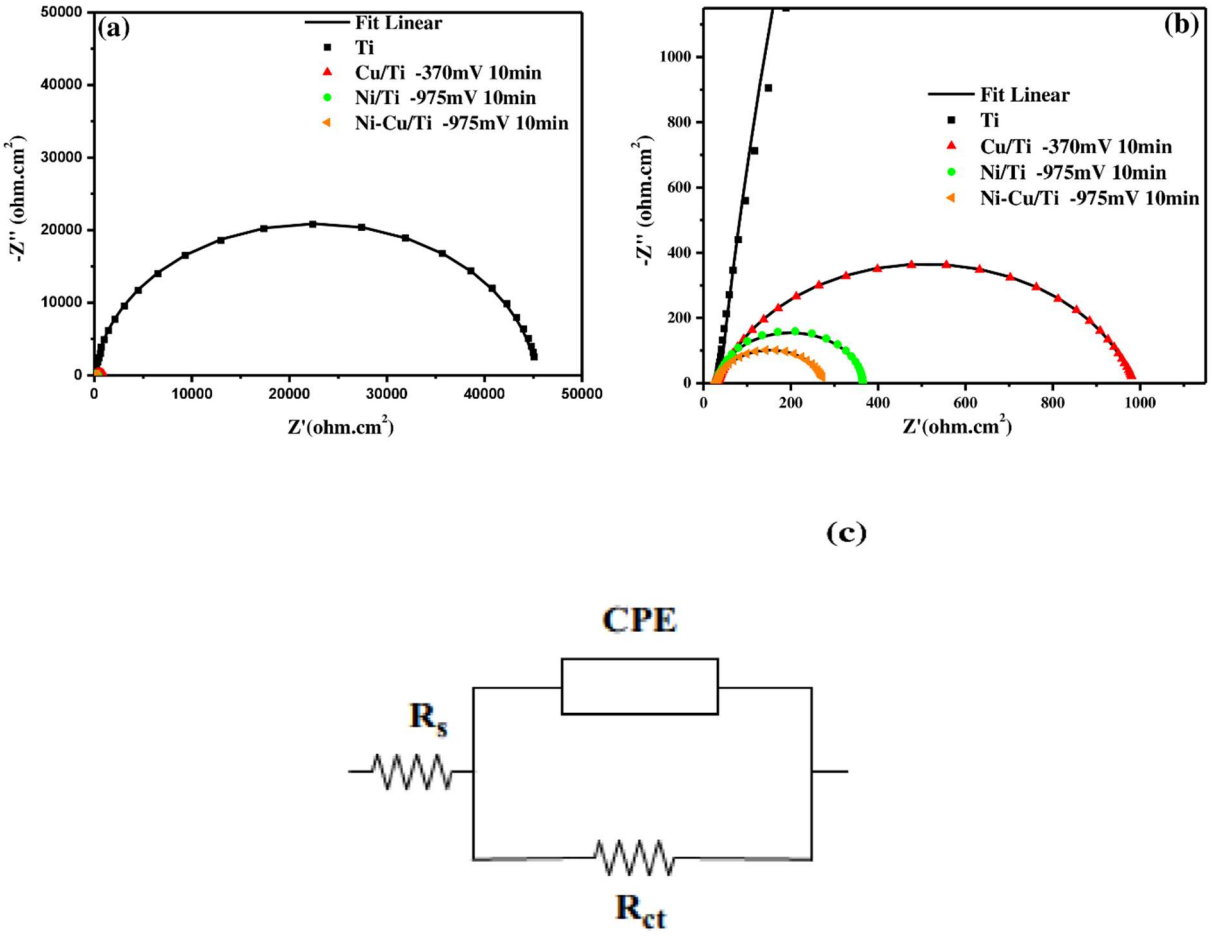
(a)
Fit Linear
Ti
Cu/Ti -370mV 10min
Ni/Ti -975mV 10min
Ni-Cu/Ti -975mV 10min
-Z'' (ohm.cm2)
Z'(ohm.cm2)
(b)
Fit Linear
Ti
Cu/Ti -370mV 10min
Ni/Ti -975mV 10min
Ni-Cu/Ti -975mV 10min
-Z'' (ohm.cm2)
Z'(ohm.cm2)
(c)
CPE
Rs
Rct

Fig.19

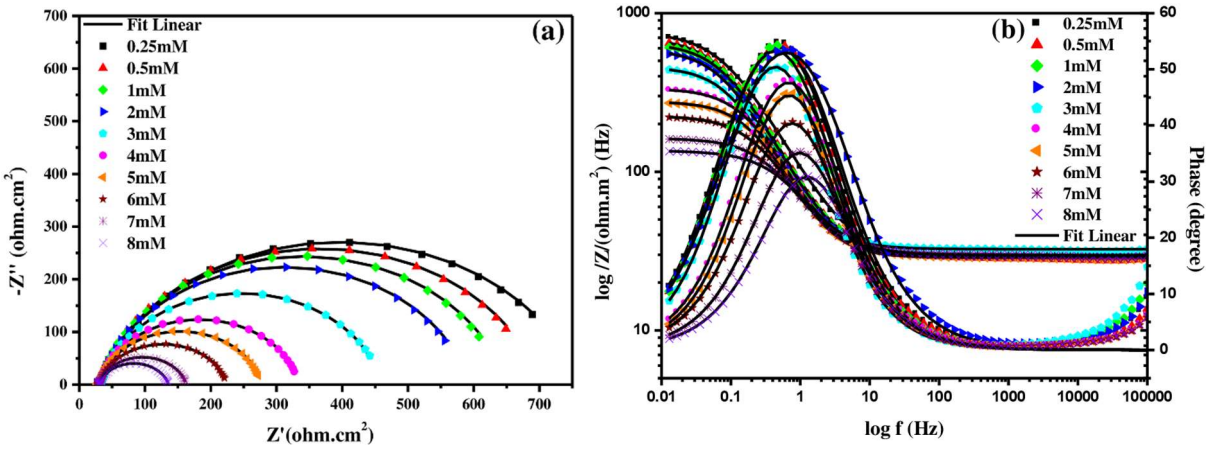
(a)
Fit Linear
0.25mM
0.5mM
1mM
2mM
3mM
4mM
5mM
6mM
7mM
8mM
-Z'' (ohm.cm2)
Z'(ohm.cm2)
(b)
0.25mM
0.5mM
1mM
2mM
3mM
4mM
5mM
6mM
7mM
8mM
Fit Linear
log /Z/(ohm.m2) (Hz)
Phase (degree)
log f (Hz)

Fig.20